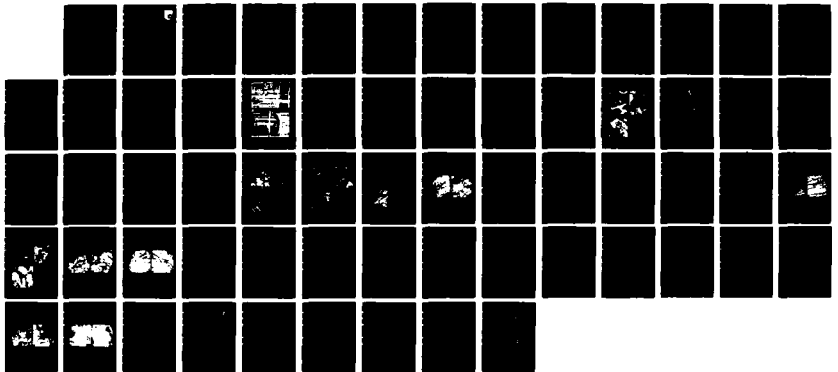


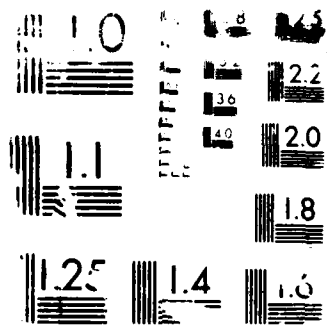
ND-A189 825

ELEVATED TEMPERATURE CRACK GROWTH STUDIES OF ADVANCED TITANIUM ALUMINIDES(U) SYSTRAM CORP DAYTON OH 1/1  
S VENKATARAMAN SEP 87 AFMAL-TR-87-4183 F33615-86-C-5142

UNCLASSIFIED

F/G 11/6.1 NL



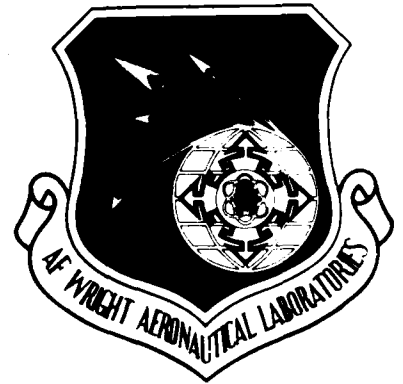


AFWAL-TR-87-4103

DTIC FILE COPY

2

AD-A189 025



ELEVATED TEMPERATURE CRACK GROWTH STUDIES OF ADVANCED  
TITANIUM ALUMINIDES

Dr. Srivathsan Venkataraman  
Systran Corporation  
4126 Linden Avenue  
Dayton, Ohio 45432

DTIC  
ELECTE  
FEB 18 1988  
S D

September 1987

Final Report for Period September 86 to April 87

Approved for public release; distribution unlimited.

MATERIALS LABORATORY  
AIR FORCE WRIGHT AERONAUTICAL LABORATORIES  
AIR FORCE SYSTEMS COMMAND  
WRIGHT-PATTERSON AIR FORCE BASE, OHIO 45433-6533

88 2 17 02!

NOTICE

When Government drawings, specifications, or other data are used for any purpose other than in connection with a definitely Government-related procurement, the United States Government incurs no responsibility or any obligation whatsoever. The fact that the Government may have formulated or in any way supplied the said drawings, specifications, or other data, is not to be regarded by implication, or otherwise in any manner construed, as licensing the holder, or any other person or corporation; or as conveying any rights or permission to manufacture, use, or sell any patented invention that may in any way be related thereto.

This report has been reviewed by the Office of Public Affairs (ASD/PA) and is releasable to the National Technical Information Service (NTIS). At NTIS, it will be available to the general public, including foreign nations.

This technical report has been reviewed and is approved for publication.

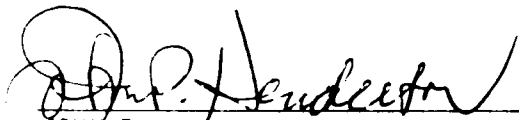


FRED W. VAHLDIEK  
Project Engineer  
Metals Behavior Branch



ALLAN W. GUNDERSON, Tech Area Mgr  
Metals Behavior Branch  
Metals and Ceramics Division

FOR THE COMMANDER



JOHN P. HENDERSON, Chief  
Metals Behavior Branch  
Metals and Ceramics Division

If your address has changed, if you wish to be removed from our mailing list, or if the addressee is no longer employed by your organization please notify AFWAL/MLLN, Wright-Patterson AFB, OH 45433-6533 to help us maintain a current mailing list.

Copies of this report should not be returned unless return is required by security considerations, contractual obligations, or notice on a specific document.

REPORT DOCUMENTATION PAGE

1a. REPORT SECURITY CLASSIFICATION Unclassified		1b. RESTRICTIVE MARKINGS None	
2a. SECURITY CLASSIFICATION AUTHORITY n/a		3. DISTRIBUTION/AVAILABILITY OF REPORT Approved for public release; distribution is unlimited.	
2b. DECLASSIFICATION/DOWNGRADING SCHEDULE n/a		5. MONITORING ORGANIZATION REPORT NUMBER(S) AFWAL-TR-87-4103	
4. PERFORMING ORGANIZATION REPORT NUMBER(S)		7a. NAME OF MONITORING ORGANIZATION Materials Laboratory, Metals Behavior Branch (AFWAL/MLLN)	
6a. NAME OF PERFORMING ORGANIZATION SYSTRAN Corporation	5b. OFFICE SYMBOL (If applicable) n/a	7b. ADDRESS (City, State and ZIP Code) AF Wright Aeronautical Laboratories Wright-Patterson AFB, OH 45433-6533	
6c. ADDRESS (City, State and ZIP Code) 4126 Linden Avenue Dayton, OH 45432		9. PROCUREMENT INSTRUMENT IDENTIFICATION NUMBER F33615-86-C-5142	
8a. NAME OF FUNDING/SPONSORING ORGANIZATION Materials Laboratory Metals Behavior Branch	8b. OFFICE SYMBOL (If applicable) AFWAL/MLLN	10. SOURCE OF FUNDING NOS	
8c. ADDRESS (City, State and ZIP Code) Wright-Patterson AFB, OH 45433-6533		PROGRAM ELEMENT NO 62102F	PROJECT NO 3005
11. TITLE (Include Security Classification) Elevated Temperature Crack Growth Studies of Advanced TiAl.		TASK NO. 50	WORK UNIT NO 92
12. PERSONAL AUTHOR(S) Dr. Srivathsan Venkataraman			
13a. TYPE OF REPORT Final Technical Rept	13b. TIME COVERED FROM 9/2/86 TO 4/24/87	14. DATE OF REPORT (Yr., Mo., Day) September 1987	15. PAGE COUNT 69
16. SUPPLEMENTARY NOTATION This is a Small Business Innovative Research Program, Phase I report.			
17. COSATI CODES		18. SUBJECT TERMS (Continue on reverse if necessary and identify by block number)	
FIELD 11	GROUP 04	SUB GR	Fatigue Crack Growth Titanium Aluminide Plus Niobium Elevated Temperature Environmental Influence Heat Treatment Fractography
19. ABSTRACT (Continue on reverse if necessary and identify by block number) <p>Ordered intermetallic titanium aluminide TiAl alloyed with niobium possesses attractive high temperature properties and moderate low temperature ductibility. Currently, its application is limited to static components in aircraft gas turbine engines. To extend their use to rotating components of turbine engines, better understanding of life limiting processes such as creep/fatigue crack growth and fracture is required.</p> <p>Phase I of this Air Force Small Business Innovative Research program involved investigation of fatigue crack growth in an alpha two titanium aluminide plus niobium alloy (titanium - 16 wt% aluminum - 10 wt% niobium) as a function of temperature and environment. Computer automated fatigue crack growth tests were conducted in both air and vacuum environments at temperatures ranging from room temperature to 1200 F (649 C). Two heat treatment conditions, namely, beta solution and alpha + beta solution resulted in coarse and fine grain materials, respectively, with varying alpha two morphology. Fractographic analyses were conducted for all test specimens. (continued on reverse side)</p>			
20. DISTRIBUTION/AVAILABILITY OF ABSTRACT UNCLASSIFIED/UNLIMITED <input checked="" type="checkbox"/> SAME AS RPT <input type="checkbox"/> DTIC USERS <input type="checkbox"/>		21. ABSTRACT SECURITY CLASSIFICATION Unclassified	
22a. NAME OF RESPONSIBLE INDIVIDUAL Fred Vahldiek		22b. TELEPHONE NUMBER (Include Area Code) 513-255-2689	22c. OFFICE SYMBOL AFWAL/MLLN

The fatigue crack growth data indicated fracture toughness values over 25 MPa m for both heat treated materials at temperatures above 600 F. Moderate increase in growth rate is observed with increase in temperature. Lowest growth rate is observed at 1000 F when tested in vacuum environment indicating a strong environmental interaction in the alpha two titanium aluminide.

Fractographic analysis revealed an increased ductility in vacuum tested samples. However, for all conditions tested only transgranular fracture morphology was observed.

(Block 19)

## FOREWORD

This report covers work performed under Air Force Small Business Innovation Research Phase I research contract F33615-86-C-5142 from September 2, 1986 through April 24, 1987.

The investigation was conducted by the SYSTRAN Corporation, Dayton, Ohio and was monitored by Mr. Fred Vahldiek of the Metals Behavior Branch, AFWAL/MLLN, Wright-Patterson Air Force Base, Ohio.

Mr. Milton Zellmer was the program manager and Dr. Srivathsan Venkataraman performed as the Principal Investigator.

Appreciation is expressed to Dr. Theodore Nicholas and Ms. Monica Stucke of AFWAL/MLLN, WPAFB for helpful discussions and to Dr. Noel Ashbaugh of the University of Dayton Research Institute for conducting fatigue crack growth tests. Secretarial assistance of Ms. Carolyn Jordan and Ms. Chris Ollinger is acknowledged. Appreciation is also extended to Mr. Gus Seefluth and Ms. Valerie Monell for their valuable assistance in the preparation of this report.

Accession For	
NTIS CRA&I	<input checked="" type="checkbox"/>
DTIC TAB	<input type="checkbox"/>
Unannounced	<input type="checkbox"/>
Justification	
By _____	
Distribution/	
Availability Codes	
Date	Accession For
A-1	Special

## TABLE OF CONTENTS

	Page
INTRODUCTION	1
EXPERIMENTAL DETAILS	5
RESULTS AND DISCUSSION	13
CONCLUSIONS AND RECOMMENDATIONS	45
REFERENCES	52



## LIST OF FIGURES

FIGURE NUMBER	DESCRIPTION	PAGE NUMBER
1	Schematic of round mini compact tension specimen. All dimensions are in inches.	6
2	Experimental set up for computer automated fatigue crack growth testing.	8
3	Load versus displacement plot and closure load measurement technique.	11
4	Illustration of manual smoothing technique.	12
5	Optical micrographs of beta solutioned (2280°F) and annealed (1141°F) Ti <sub>3</sub> Al alloy. Kröll's etchant.	14
6	Optical micrographs of alpha & beta solutioned (2050°F) and annealed (1141°F) Ti <sub>3</sub> Al alloy. Kröll's etchant.	15
7	Fatigue crack growth data obtained for Ti <sub>3</sub> Al at the temperature of 1200°F.	17
8	Closure data obtained for Ti <sub>3</sub> Al at the temperature of 1200°F in air environment.	18
9	Closure data obtained for Ti <sub>3</sub> Al at the temperature of 1200°F in vacuum environment.	19
10	Closure corrected fatigue crack growth data for Ti <sub>3</sub> Al obtained at the temperature of 1200°F.	20
11	SEM fractographs of beta solutioned Ti <sub>3</sub> Al fatigue crack growth specimen tested in air at 1200°F.	22
12	SEM fractographs of beta solutioned Ti <sub>3</sub> Al fatigue crack growth specimen tested in vacuum at 1200°F.	23
13	SEM fractographs of alpha & beta solutioned Ti <sub>3</sub> Al fatigue crack growth specimen tested in air at 1200°F.	24

FIGURE NUMBER	DESCRIPTION	PAGE NUMBER
14	SEM fractographs of alpha & beta solutioned $Ti_3Al$ fatigue crack growth specimen tested in vacuum at 1200°F.	25
15	Fatigue crack growth data obtained for $Ti_3Al$ at the temperature of 1000°F.	27
16	Closure data obtained for $Ti_3Al$ at the temperature of 1000°F in air environment.	28
17	Closure data obtained for $Ti_3Al$ at the temperature of 1000°F in vacuum environment.	29
18	Closure corrected fatigue crack growth data for $Ti_3Al$ obtained at the temperature of 1000°F.	30
19	SEM fractographs of beta solutioned $Ti_3Al$ fatigue crack growth specimen tested in air environment at 1000°F.	31
20	SEM fractographs of beta solutioned $Ti_3Al$ fatigue crack growth specimen tested in vacuum at 1000°F.	32
21	SEM fractographs of alpha & beta solutioned $Ti_3Al$ fatigue crack growth specimen tested in air at 1000°F.	33
22	SEM fractographs of alpha & beta solutioned $Ti_3Al$ fatigue crack growth specimen tested in vacuum at 1000°F.	34
23	Fatigue crack growth data obtained for $Ti_3Al$ at the temperature of 800°F.	36
24	Fatigue crack growth data obtained for $Ti_3Al$ at the temperature of 600°F.	37
25	Closure data obtained for $Ti_3Al$ at the temperature of 800°F in air environment	38
26	Closure data obtained for $Ti_3Al$ at the temperature of 600°F in air environment.	39
27	Closure corrected fatigue crack growth data for $Ti_3Al$ obtained at the temperature of 800°F.	40

FIGURE NUMBER	DESCRIPTION	PAGE NUMBER
28	Closure corrected fatigue crack growth data for $Ti_3Al$ obtained at the temperature of 600°F.	41
29	Fatigue crack growth data obtained for $Ti_3Al$ at the temperature of 75°F (room temperature).	42
30	Closure data obtained for $Ti_3Al$ at the temperature of 75°F (room temp.) in air environment.	43
31	Closure corrected fatigue crack growth data for $Ti_3Al$ obtained at the temperature of 75°F (room temp.).	44
32	SEM fractographs of beta solutioned $Ti_3Al$ fatigue crack growth specimen tested in air environment at 75°F (room temp.).	46
33	SEM fractographs of alpha & beta solutioned $Ti_3Al$ fatigue crack growth specimen tested in air at 75°F (room temp.).	47
34	Summary of fatigue crack growth data obtained for the beta solutioned $Ti_3Al$ over a temperature range of 75° to 1200°F in both air and vacuum environment.	48
35	Summary of fatigue crack growth data obtained for the alpha & beta solutioned $Ti_3Al$ over a temperature of 75° to 1200°F in both air and vacuum environment.	49

## INTRODUCTION:

Improvements in high performance aircraft gas turbine engine designs require materials that can operate at increasingly higher temperatures over long periods of time while still retaining adequate mechanical and corrosion properties. Materials of high strength and light weight (low density) are essential to meet these requirements. In the past, major advances in engine technology have been made using nickel and cobalt base superalloys and the conventional alpha-beta titanium alloys. With the anticipated future engine design requirements surpassing the capabilities of these materials, there is a need for the development of new classes of materials with superior mechanical and corrosion properties. Intermetallic compounds or ordered alloys are particularly suited to these needs.

In general, these intermetallic compounds exhibit properties which lie between conventional metallic alloys and ceramics in that they have limited ductility and attractive high temperature strength. A compound of great interest and potential under this category is the alpha-two titanium aluminide ( $Ti_3Al$ ). This compound has been extensively studied in the USA by Air Force Materials Laboratory and major engine manufacturers<sup>1,2</sup> as well as in the USSR<sup>3,4</sup>. Preliminary design analysis and payoff studies made for these materials indicated significant weight savings in a wide range of engine applications, such as an advanced transport engine (ATE), an advanced tactical fighter engine (ATF), or an advanced supersonic transport engine (AST)<sup>2</sup>. Turbine rotor weight savings from 30 to 40% (3 to 5% of engine weight) could be achieved with widespread application of the titanium aluminide in rotating hardware, or engine weight savings of up to 16% could be achieved by its application in static structures such as vanes, cases and bearing supports.

Besides these advantages, another major area of benefit in application of this material relates to the growing problem of availability of strategic materials. The majority of current known reserves of elements necessary for superalloys are controlled by foreign sources. The chromium supply, which is a critical requirement in conventional superalloys, depends heavily on sources such as USSR and Turkey while Mainland China possesses the majority of the world supply of tungsten. Whereas, the United States has an enormous domestic reserve of titanium which can further be supplemented from other friendly sources such as Australia and Canada. Thus, the successful use of the titanium aluminide in gas turbine engines would reduce the United States dependence on foreign sources for superalloy constituent elements, and would potentially reduce high temperature material costs at the same time.

The intermetallic alpha two titanium aluminide ( $Ti_3Al$ ) is known to order as the  $DO_{19}$  superlattice. This ordered intermetallic compound is stiffer than conventional titanium alloys and its static strength and stiffness do not degrade very rapidly with increasing temperatures.<sup>5</sup> Modulus retention with temperature in this material is particularly high because of the strong A-B bonding.<sup>1</sup> In addition, a number of high temperature properties which depend on diffusive mechanisms are improved because of the generally high activation energy required for diffusion in ordered alloys. Alpha two titanium aluminide has excellent oxidation resistance due to a large aluminum content.<sup>6</sup> Further, this ordered alloy has adequate creep strength at high temperatures.<sup>7</sup> The limited ductility of these aluminides has also been improved through alloy additions such as niobium and tungsten which has enabled better processing techniques such as casting of large ingots and forging to form sheet bar.<sup>8</sup>

In spite of the superior properties of titanium aluminide, at present

they are used essentially in static parts of the advanced Air Force gas turbine engines. Thorough understanding of the life limiting processes such as fatigue crack growth and fracture at elevated temperatures occurring in this new class of advanced structural alloy is essential for extending its application to moving engine components.

The limited ductility of alpha two titanium aluminide plays an important role in the fatigue crack growth behavior of this alloy. Little information is available in open literature about the crack growth behavior of the alloy under various combinations of loading and environment. The crack growth process generally depends on various parameters such as temperature, frequency, load amplitude, wave shape, hold time, environment, etc. Other consequential aspects also include threshold behavior, crack closure, short crack behavior, etc.

Crack growth rate calculations for critical structural components in US Air Force gas turbine engines under actual operating conditions are necessary for design and life management procedures. Programs such as Retirement-for-cause (RFC) and Air Force Engine Structural Integrity Program (ENSIP) require life prediction analysis based on crack growth rates calculated from initial flaw sizes using fracture mechanics concepts. In the past, such predictions of crack growth has been generally approached through the study of the basic phenomena of crack growth associated with cyclic and sustained loading under conditions of temperature and environment representative of engine operations.<sup>9</sup> With the addition of interaction effects, the results of these fundamental studies have been collected to address crack growth in the specific engine spectrum and provide more meaningful life prediction methods for components. This research program follows a similar concept of crack growth studies on

laboratory scale specimens made of ordered titanium aluminide alloy to determine the suitability of this material as well as to develop life prediction methodology for its applications in various rotating engine components.

To evaluate the feasibility of this concept for this material, a well characterized alpha two ordered titanium aluminide alloy of composition titanium - 16 wt% aluminum - 10 wt% niobium (titanium - 25 atom% aluminum - 5 atom% niobium) was chosen to study the influence of the environment, temperature (ductility) and microstructural features on the fatigue crack growth rate, fracture mode and associated micromechanisms. This report presents the results obtained during this investigation conducted under the Air Force Small Business Innovation Research Phase I program.

## EXPERIMENTAL DETAILS

Powder titanium - 16 wt% aluminum - 10 wt% niobium alloy was produced by the rotating electrode process, canned, hot compacted and subsequently extruded at 2200°F (1204°C). The extrusion ratio was selected at 6:1. Sections of the extruded bar were solutioned in either beta phase field at 2280°F (1249°C) or alpha plus beta field at 2050°F (1121°C) for one hour and air cooled to room temperature. Solutioned bars were then aged at 1441°F (800°C) for eight hours and air cooled. Heat treatment details are given in Table I.

TABLE I  
HEAT TREATMENT SCHEDULE

#	Solution Details				Anneal Details		
	Phase Field	Temperature °F/°C	Time Hrs	Cooling medium	Temperature °F/°C	Time Hrs	Cooling medium
1	Beta	2280/1250	1	Air	1441/800	8	Air
2	Alpha+Beta	2050/1121	1	Air	1441/800	8	Air

Round mini compact tension type specimens of the dimensions shown in Figure 1 were machined from heat treated sections using an electron discharge milling technique. Machining was carried out at Metcut Research, Cincinnati, Ohio. Specimen surfaces were metallographically polished down to 3 micron finish to enable optical crack length monitoring.

Constant load amplitude fatigue crack growth tests were conducted in both air and vacuum atmospheres at temperatures ranging from room temperature to 1200°F (649°C). Tests in air atmosphere were done at the University of Dayton Research Institute, Dayton, Ohio.

All these fatigue crack growth tests were carried out in an automated



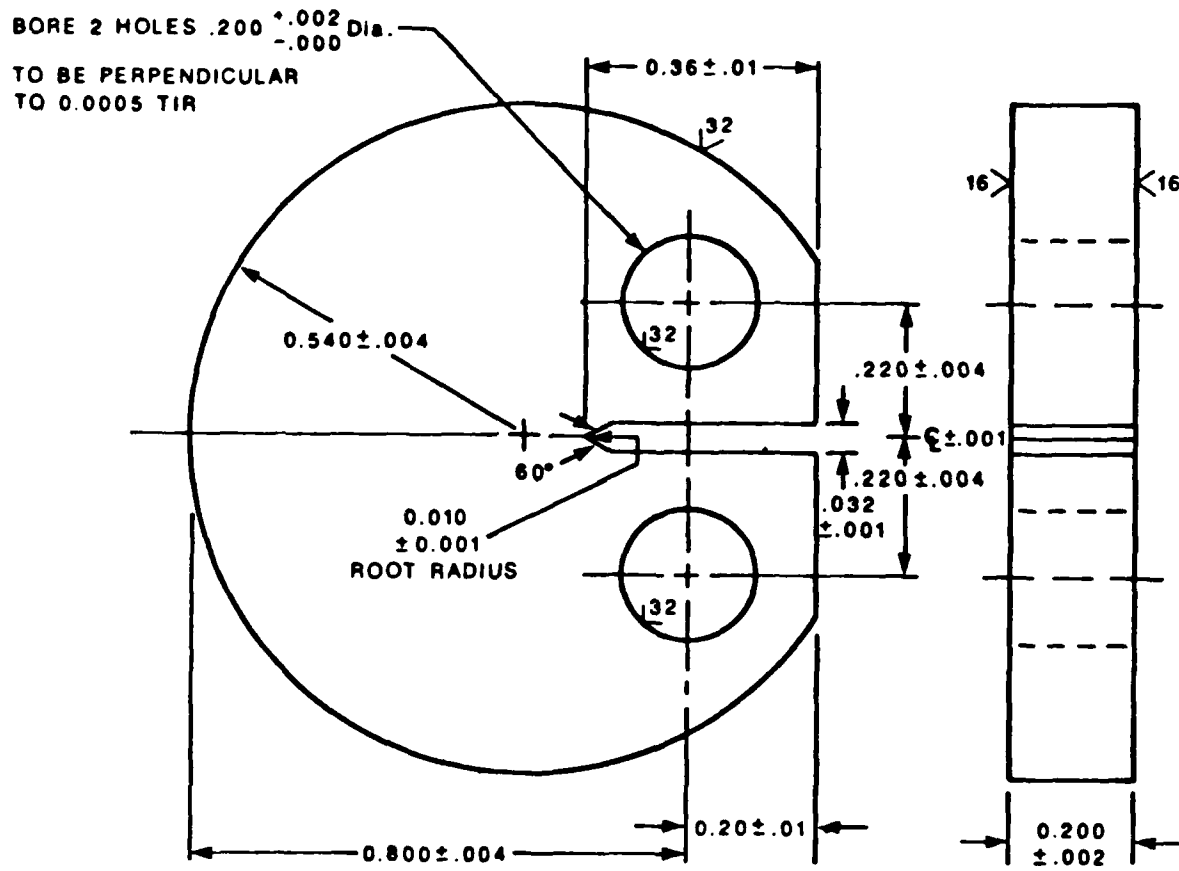


Figure 1 Schematic of round mini compact tension specimen.  
 All dimensions are in inches.

servo-hydraulic testing machine under computer control. The specimen was maintained at constant temperature in a resistance heated oven having windows through which optical surface crack length could be periodically monitored with the aid of a travelling microscope, Figure 2. The primary crack length data were obtained from compliance measurements from load-displacement data. Crack mouth opening displacements were obtained with the aid of an extensometer with quartz rod extension arms. The extensometer was mounted outside the oven. Compliance was determined from a least squares linear regression to the unloading portion of the digital load-displacement data over a range from 95% maximum load to a lower window (generally around 50% maximum load), which is above the closure load. The compliance determined crack lengths were verified through optical surface crack length measurements.

For testing under vacuum environment, the oven as well as the extensometer assembly were placed inside a vacuum chamber made of stainless steel. A turbomolecular pumping system was used to attain the vacuum in the range of  $10^{-6}$  torr. Molybdenum resistance heating elements were used in the oven along with tantalum heat shields. These materials absorb oxygen efficiently at elevated temperatures, further reducing the oxygen partial pressure in the specimen zone than the vacuum levels would reflect.

As a first step, precracking was conducted for all specimens at test temperatures following the ASTM standard E647. Sinusoidal load waveforms with a frequency of 1 Hz and a minimum to maximum load ratio (R) of 0.1 were utilized for precracking.

For constant load amplitude tests, again a sinusoidal load wave form with a frequency of 1 Hz and a load ratio of 0.1 was used. A load amplitude was selected for each test and was maintained constant. As a

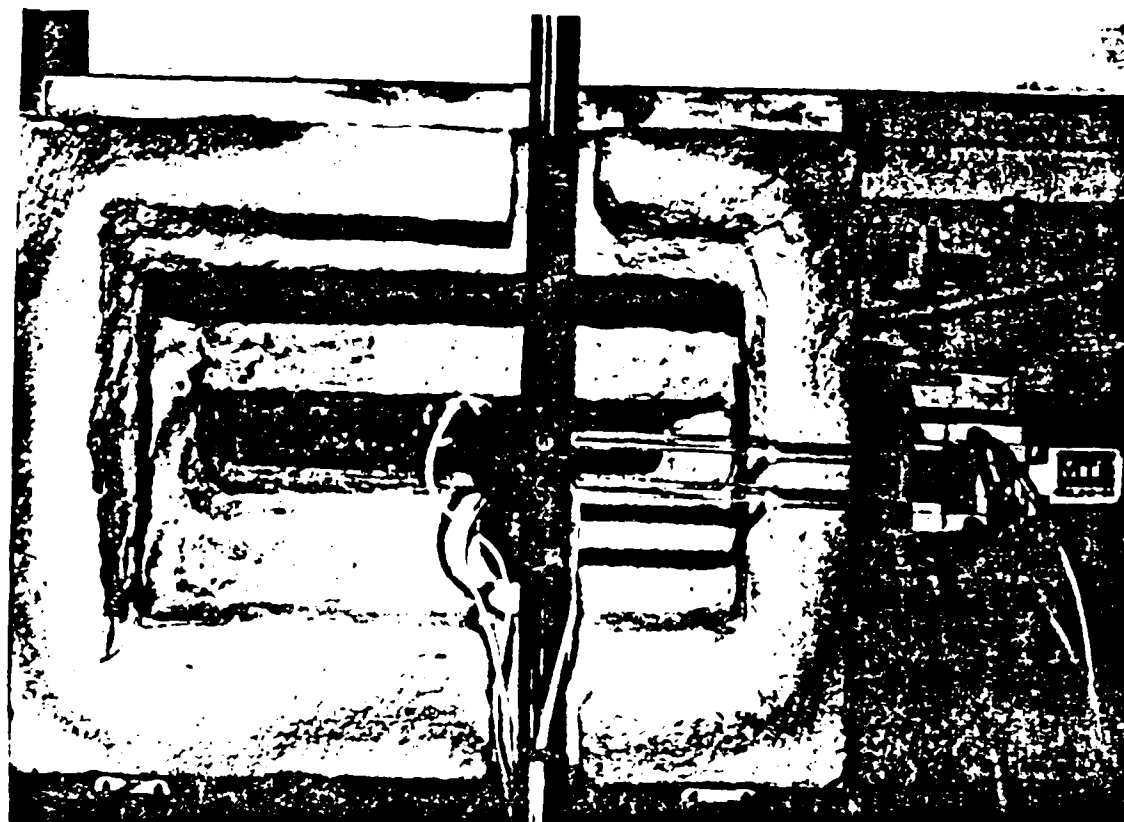
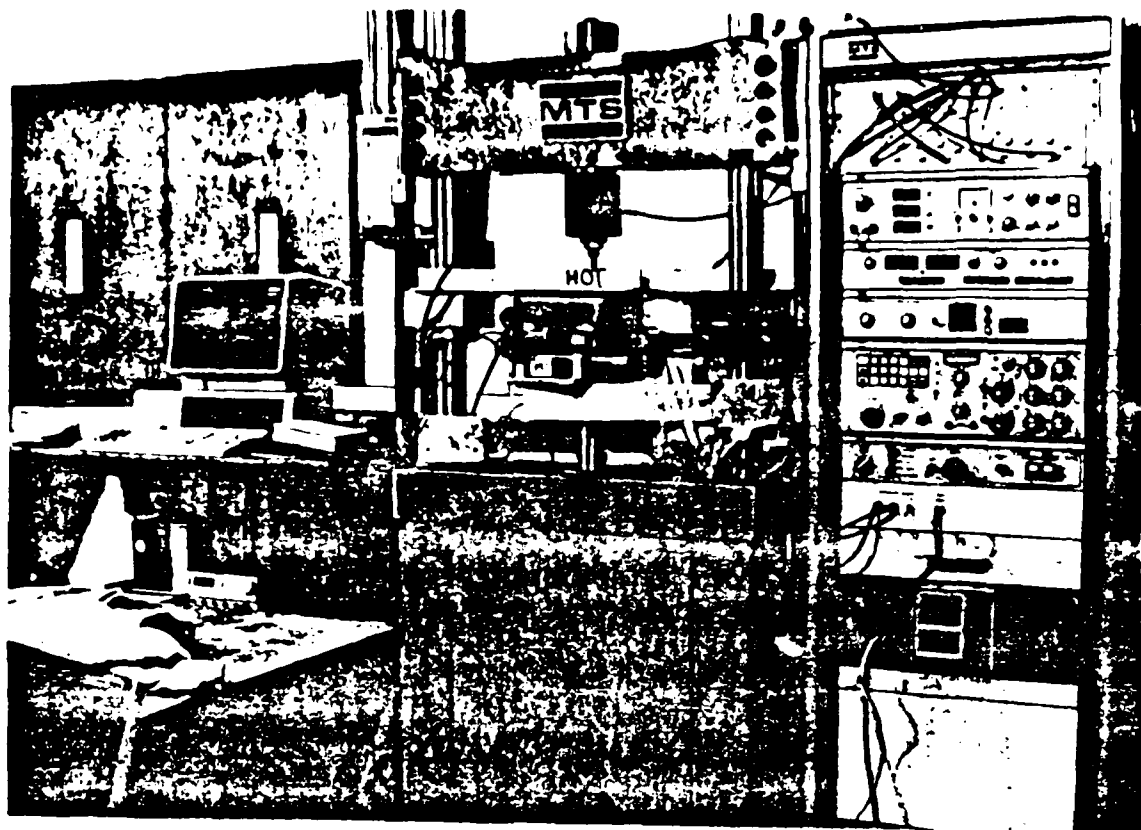


Figure 2 Experimental set up for computer automated fatigue crack growth testing.

result, the stress intensity range ( $\Delta K$ ) increased with increasing crack length. This enabled measuring the crack growth rates at various stress intensity ranges. All test conditions are listed in Table II.

Closure measurements were made during all of the above mentioned tests. At set intervals, traces of load versus displacement and load versus differential displacement were recorded. The latter provided improved resolution for the determination of crack opening load ( $S_{op}$ ). Crack opening load values were determined from the loading portion of the fatigue cycle using an intercept method which defines the  $S_{op}$  load at the intersection of the slope lines drawn along the two linear sections of the load-differential displacement plot as shown in Figure 3.

The fatigue crack growth data for the constant load amplitude tests were reduced to the form of crack growth rate per cycle ( $da/dN$ ) versus stress intensity range ( $\Delta K$ ) using a modified incremental polynomial method.<sup>10</sup> In this procedure, all crack length data falling within a crack length interval ( $\Delta a_{reg}$ ) are fitted with a second degree polynomial, and  $da/dN$  and  $\Delta K$  are calculated at the midpoint of the interval. This process is repeated with the sliding regression being successively incremented by an amount of  $\Delta a_{inc}$ . Values of 1.524 and 0.254 mm were used for  $\Delta a_{reg}$  and  $\Delta a_{inc}$ , respectively. This procedure limits the scatter normally obtained using an ASTM standard seven point polynomial, especially below the 'knee' portion of  $da/dN$  versus  $\Delta K$  plots. The  $da/dN$  versus  $\Delta K$  plots were further smoothed manually as indicated in Figure 4 for ease of comparison.

Small sections of heat treated bars were also prepared metallographically and etched in Kroll's reagent (100 ml  $H_2O$ , 2 - 6 ml  $HNO_3$ , 1 - 3 ml HF) to reveal underlying microstructures which were then studied using an optical microscope.

To understand the mechanism of fatigue crack growth in all these

**TABLE II**  
**FATIGUE CRACK GROWTH TEST DETAILS**

Test frequency = 1.0 Hz

Test Load Ratio = 0.1

#	ID	Heat Treatment	Temperature F/ C	Environment	Maximum Load lbs
1	S87-16	Beta soln.	1200/649	Air	250
2	S87-24	Beta soln.	1200/649	Air	250
3	S87-25	Beta soln.	1200/649	Air	360
4	S87-18	Beta soln.	1000/538	Air	250
5	S87-26	Beta soln.	1000/538	Air	410
6	S87-20	Beta soln.	800/426	Air	250
7	S87-27	Beta soln.	800/426	Air	415
8	S87-21	Beta soln.	600/316	Air	275
9	S87-22	Beta soln.	75/ 24	Air	320
10	S87-23	Beta soln.	75/ 24	Air	255
11	S87-17	Beta soln.	1200/649	Vac	250
12	S87-19	Beta soln.	1000/538	Vac	350
13	S87-03	Alpha+Beta soln.	1200/649	Air	250
14	S87-07	Alpha+Beta soln.	1200/649	Air	270
15	S87-05	Alpha+Beta soln.	1000/538	Air	250
16	S87-08	Alpha+Beta soln.	800/426	Air	250
17	S87-06	Alpha+Beta soln.	600/316	Air	250
18	S87-09	Alpha+Beta soln.	75/ 24	Air	250
19	S87-04	Alpha+Beta soln.	1200/649	Vac	250
20	S87-11	Alpha+Beta soln.	1000/538	Vac	320

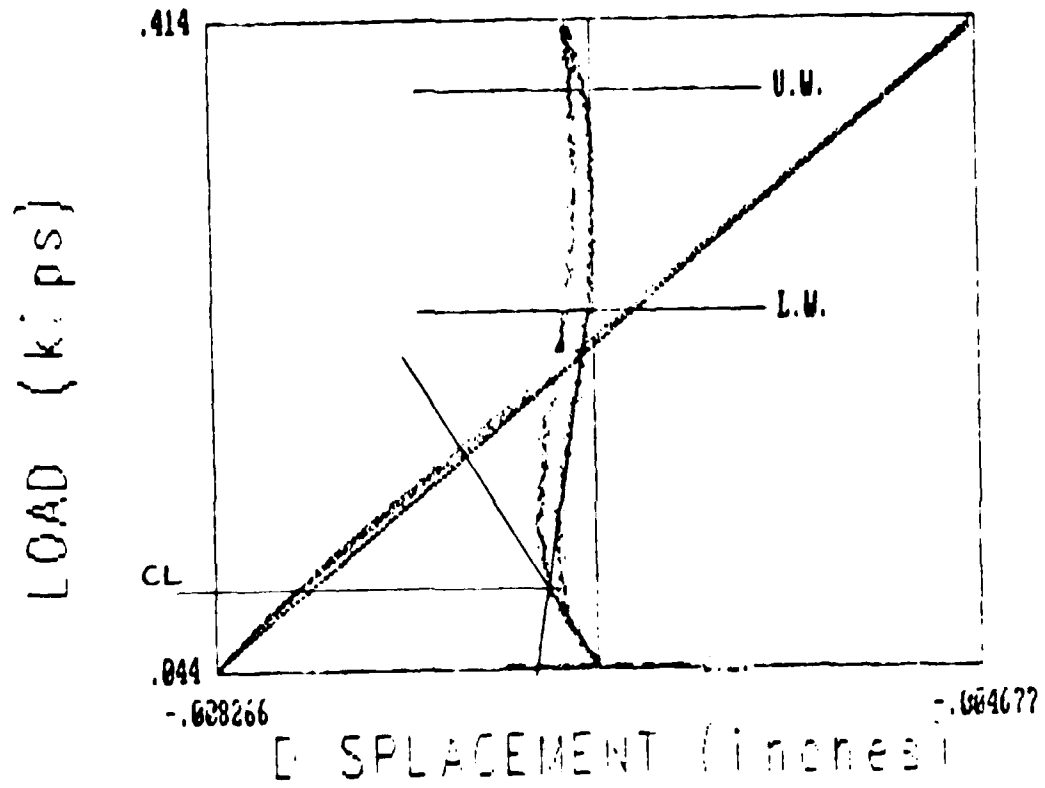


Figure 3 Load versus displacement plot and closure load measurement technique.

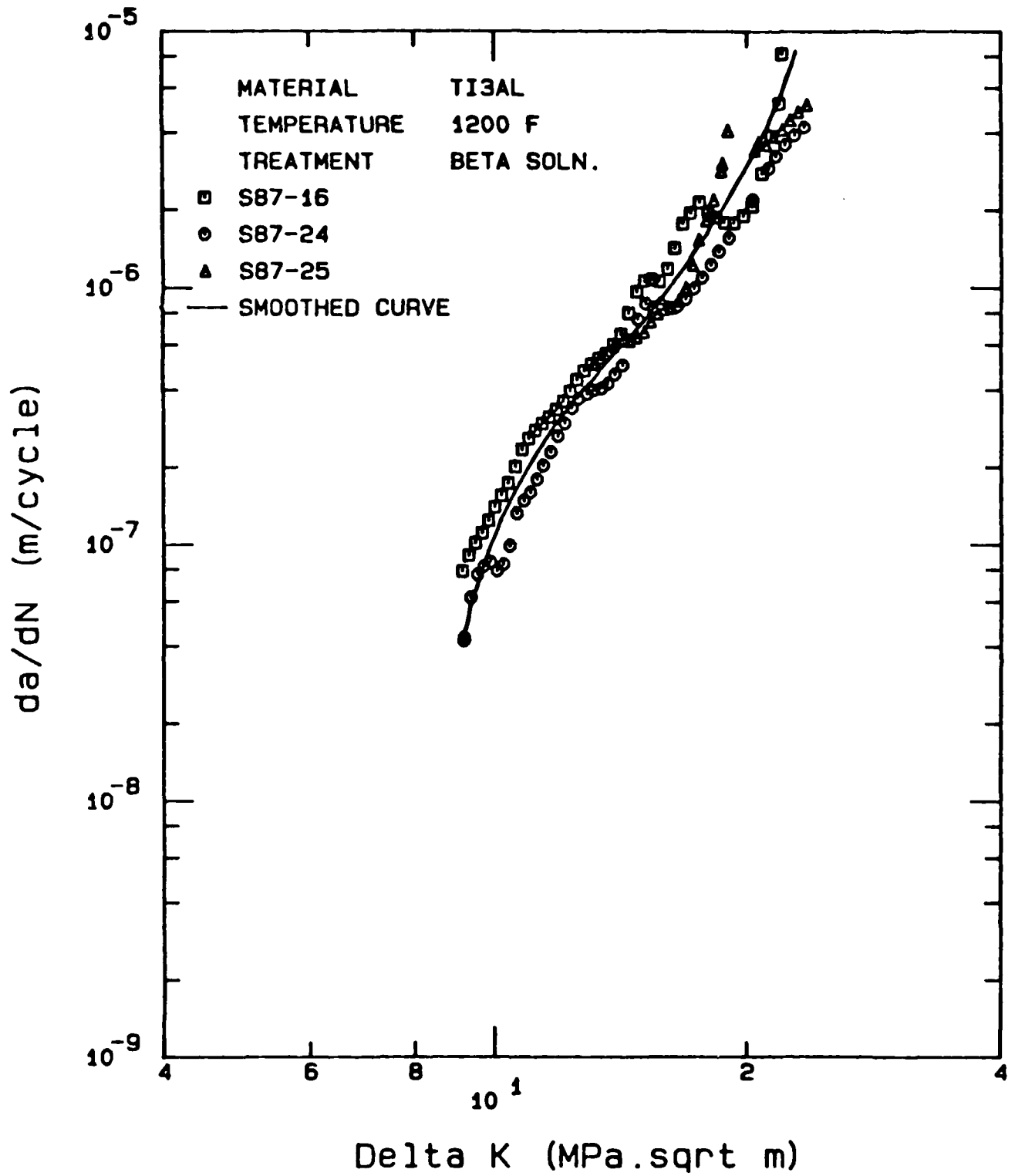


Figure 4 Illustration of manual smoothing technique.

materials, detailed fractographic analyses were carried out on all fractured test specimens using a scanning electron microscope.

## RESULTS AND DISCUSSION

Typical microstructures of the alpha two titanium aluminide solutioned at beta ( $\beta$ ) and alpha + beta ( $\alpha + \beta$ ) phase fields and annealed at 1441°F (800 °C) are presented in Figures 5 and 6. They all consist of single phase alpha two structure. The beta solution treatment results in large prior beta grain size well over 1000  $\mu$ m in diameter, as shown in Figure 5a. In Ti<sub>3</sub>Al - niobium alloys, cooling from beta phase field results in fine martensitic alpha prime phase. This is due to the beta stabilizing effect of niobium which results in a lower M<sub>s</sub> temperature thus leading to a growth limited formation of martensite plates.<sup>8</sup> Further annealing of this structure in the alpha two field (800°C) results in the fine scale sub grain structure as indicated in Figure 5b and 5c. The prior beta grain boundaries are well defined with different alpha two morphology.

Alpha + beta solution treatment, on the other hand, results in a much finer grain size as shown in Figure 6a and 6b. The grain boundaries are not well defined except for the alpha two pocket morphology seen in Figure 6c. Cooling from alpha + beta phase field results in a structure with fine acicular martensite (alpha prime formed from beta) plus transformed alpha phase. This structure, after annealing in the alpha two field, transforms to a mixture of fine subgrain structure (from martensite) and the transformation product from alpha phase. Hence, the two heat treatments provide materials with varying grain size and microstructural morphologies.

The fatigue crack growth data ( $da/dN$  vs  $\Delta K$ ) obtained at the temperature of 1200°F (649°C) in air and vacuum environment are presented





Figure 5 Optical micrographs of beta solutioned (2280°F) and annealed (1141°F) Ti<sub>3</sub>Al alloy. Kroll's etchant.

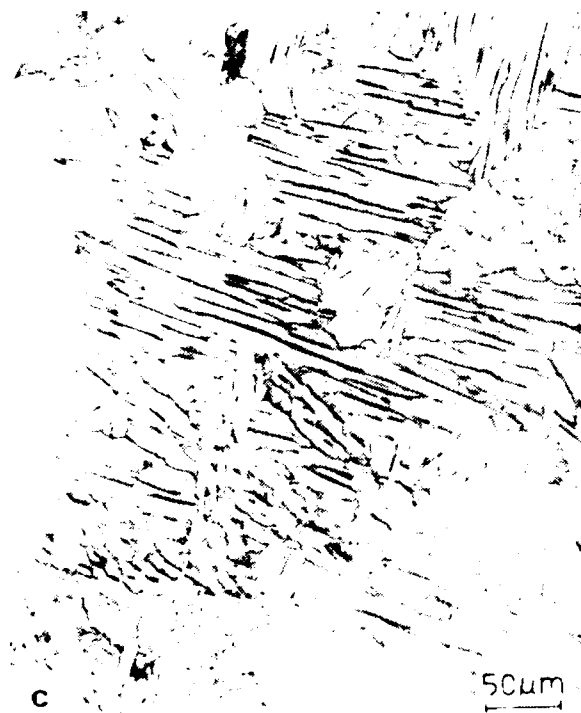
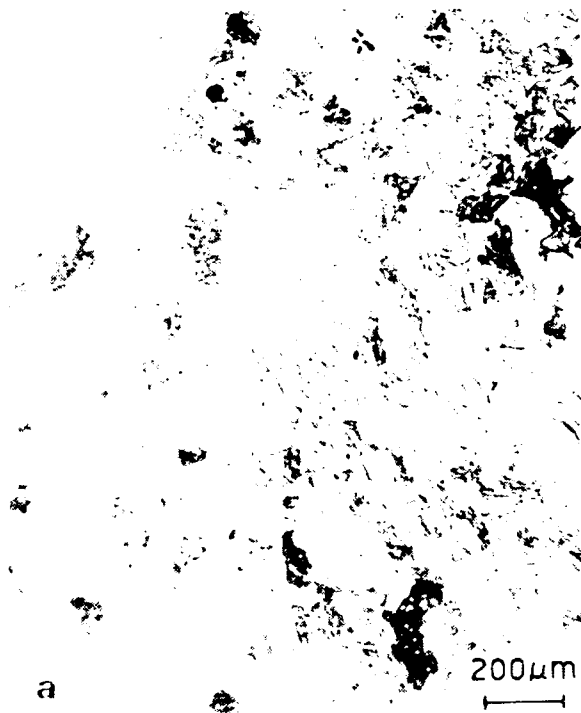


Figure 6 Optical micrographs of alpha + beta solutioned (2050 F) and annealed (1141°F) Ti<sub>3</sub>Al alloy. Kroll's etchant.

in Figure 7 for both heat treated materials. The data exhibit identical crack growth rates for both heat treatment conditions when tested in air. In vacuum environment, however, the beta solution treated material showed lower crack growth rates when compared to the fine grained alpha + beta solutioned materials. Further, for both heat treatment cases, crack growth rate at any given stress intensity range is higher in air by over an order of magnitude in comparison to that in vacuum medium.

The nature of crack growth data shown in Figure 7 indicates fracture toughness values over  $25 \text{ MPa}\sqrt{\text{m}}$  for this material. This is due to an increase in the ductility of the material at this temperature resulting from a significant activity of non-basal slip.<sup>8</sup>

The closure data ( $K_{\text{opening}}$  vs  $K_{\text{max}}$ ) obtained from the above mentioned tests are presented in Figures 8 and 9. Higher level of closure is observed for beta solutioned alloy in comparison to the alpha + beta solutioned material. This may be due to an increased level of roughness induced closure resulting from the coarse grain structure of the alloy. The predominant mechanism of roughness induced closure is further confirmed by the closure data obtained in vacuum. A plasticity induced closure mechanism is also operative at higher stress intensity ranges, indicated by a corresponding increase in the crack opening stress intensity ( $K_{\text{op}}$ ) levels. Meanwhile, the closure levels are not high enough to have a major influence on the crack growth data as shown in Figure 10. The  $da/dN$  vs  $\Delta K_{\text{effective}}$  plot shows a lower  $\Delta K_{\text{effective}}$  threshold for beta solutioned alloy. Decreasing stress intensity threshold tests should be conducted for these materials to confirm this observation. This will be carried out during the Phase II program. The growth rates in vacuum are still lower by an order of magnitude in comparison to that in air, which strongly

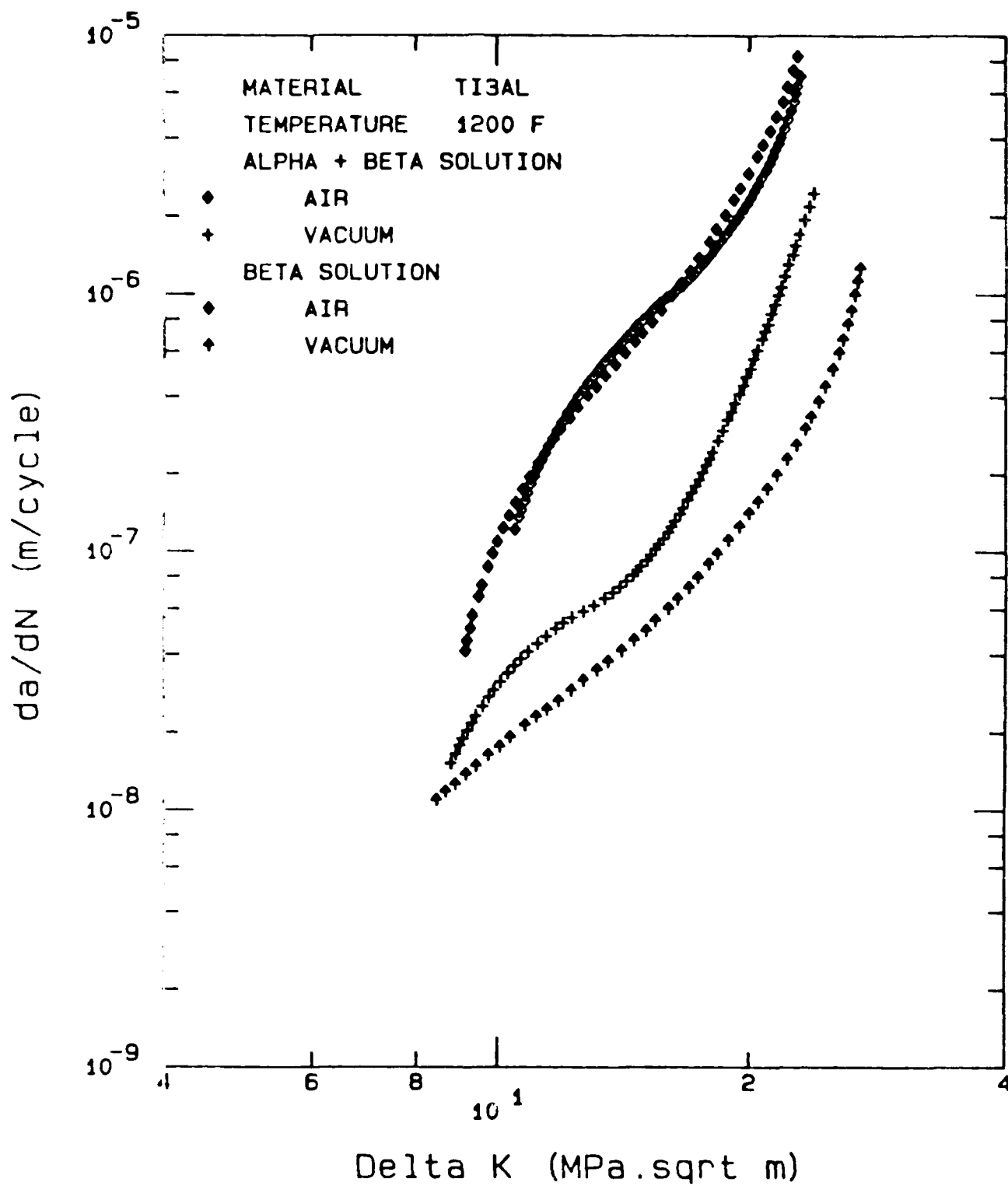


Figure 7 Fatigue crack growth data obtained for  $Ti_3Al$  at the temperature of 1200°F.

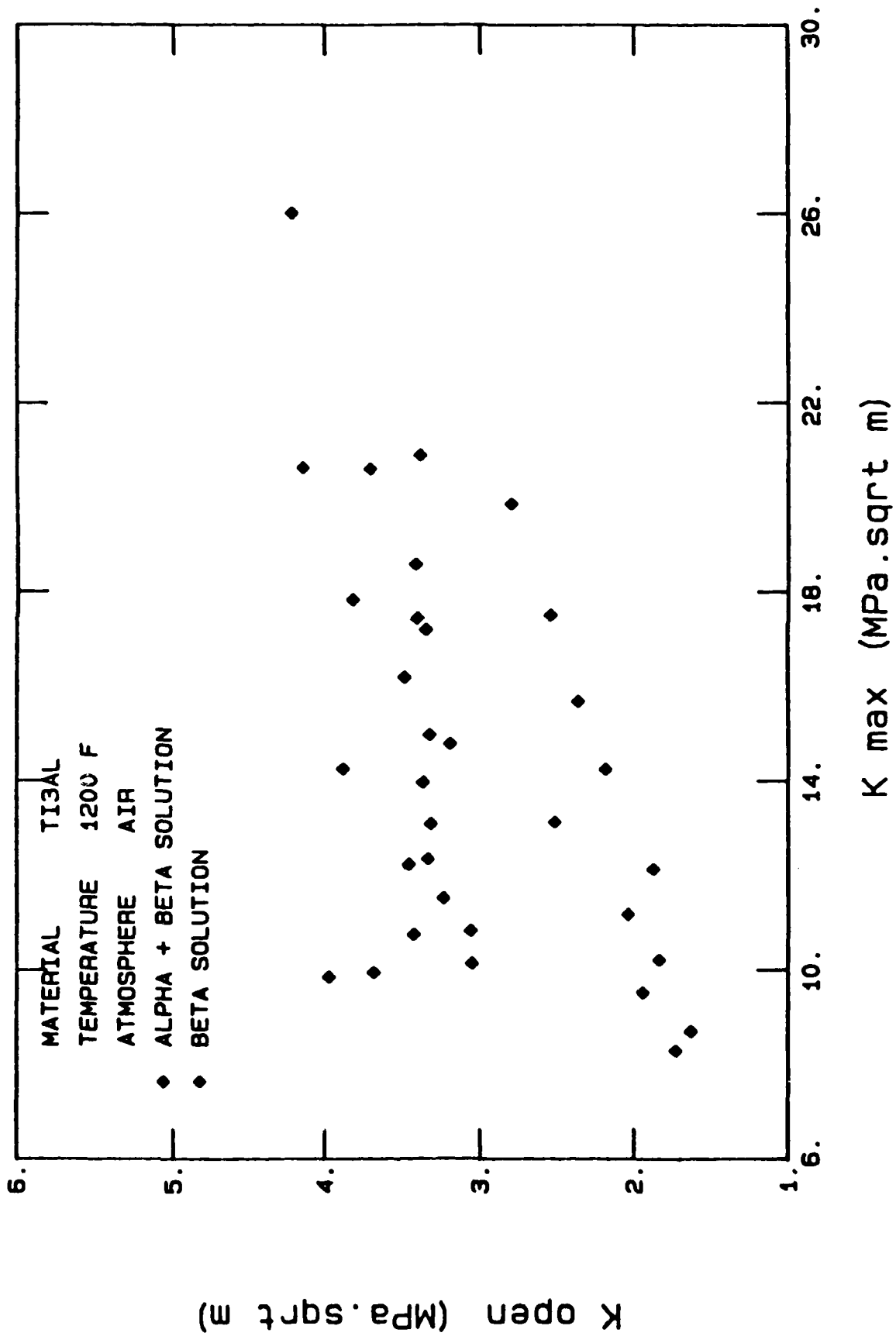


Figure 8 Closure data obtained for Ti<sub>3</sub>Al at the temperature of 1200°F in air environment.

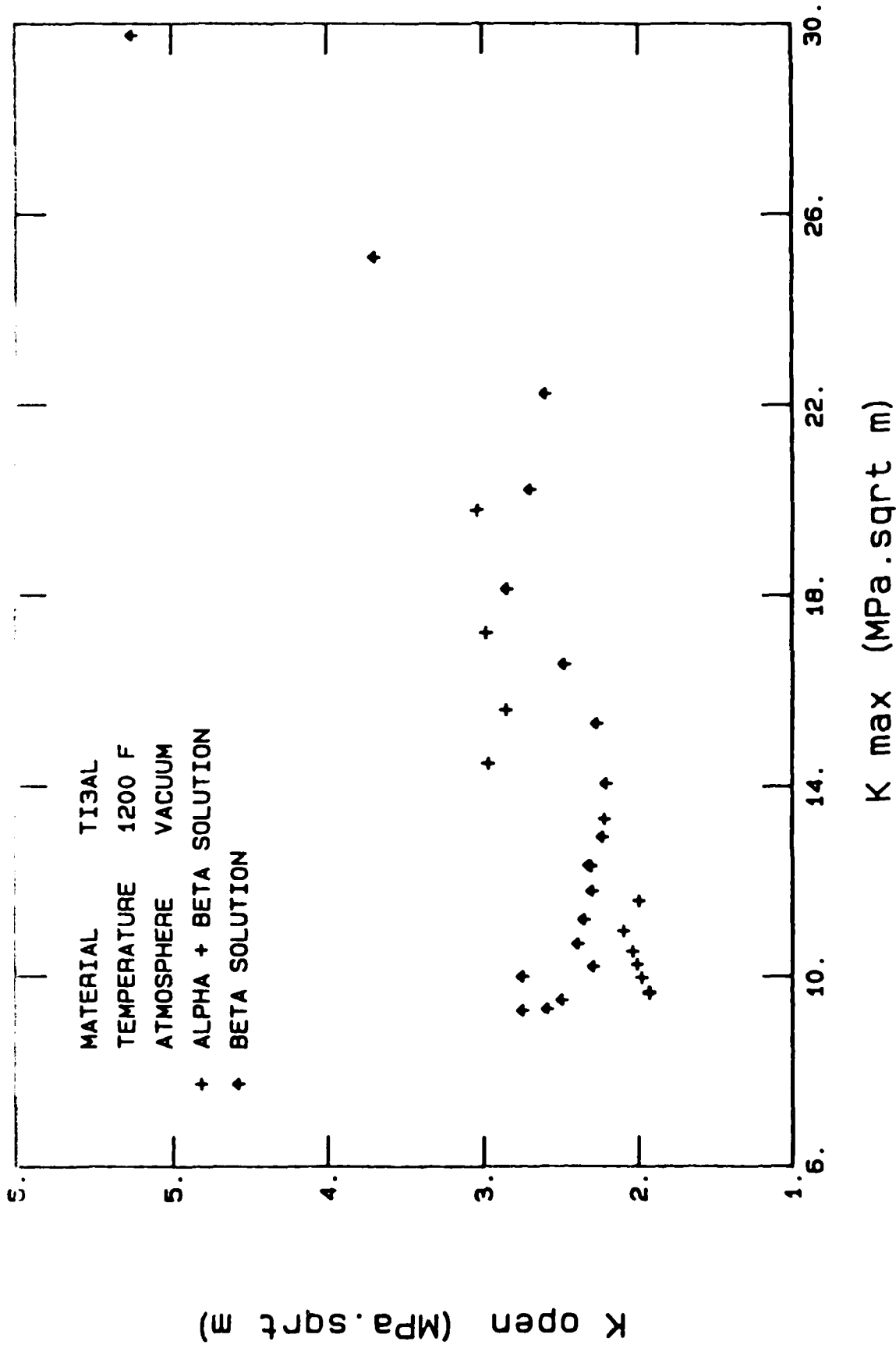


Figure 9 Closure data obtained for Ti<sub>3</sub>Al at the temperature of 1200°F in vacuum environment.

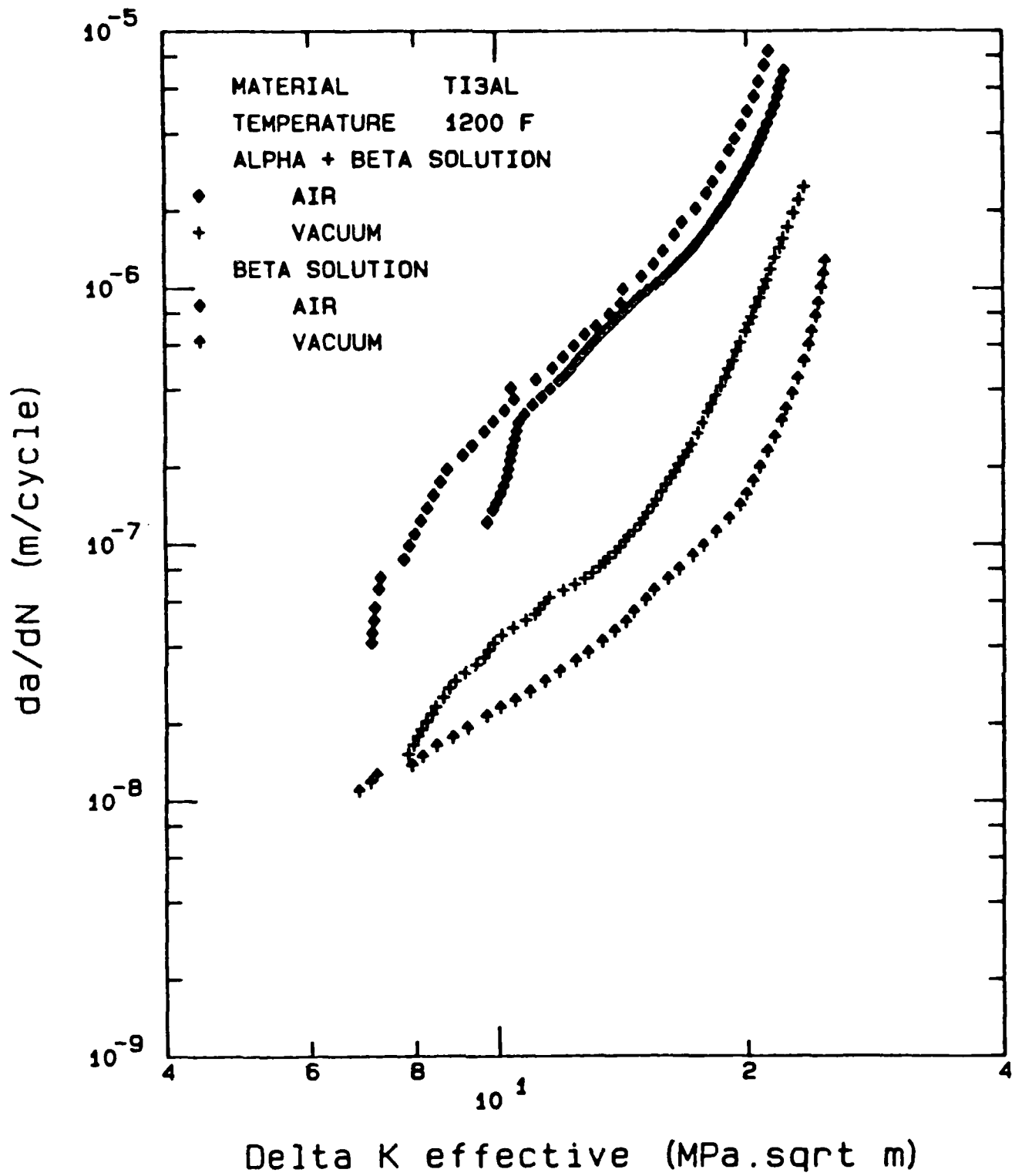


Figure 10 Closure corrected fatigue crack growth data for  $Ti_3Al$  obtained at the temperature of 1200°F.

indicates an embrittlement of these materials at elevated temperature by oxygen present in the air. Thus, application of protective coatings to these materials may be beneficial when using them at high temperatures in an oxidizing environment.

Further, crack growth rate in air and vacuum environments tend to converge at high  $\Delta K$  levels, where the crack growth kinetics supersedes the oxidation (embrittlement) kinetics in the material ahead of the crack front.

Figures 11 through 14 show the fracture appearance of both heat treated materials tested at 1200°F (649°C). The fracture morphology is predominantly cleavage in both cases when tested in air. The beta solutioned material shows large grain features as well as grain boundary cracking as seen in Figure 11a. The cleavage fracture morphology within grains is indicated by the characteristic river pattern as shown in Figure 11b. Striation-like features are also observed in isolated areas as seen in Figure 11c. However, Figures 12a and 12b show a considerable amount of surface plasticity for the vacuum tested specimen indicating an increased material ductility. In fact, a strong relationship between environment and material ductility has been observed in the past in another intermetallic compound, nickel aluminide.<sup>11</sup> Similar data for the titanium aluminide are also essential for understanding the various failure mechanisms operating in this material. This will be addressed in the Phase II program. The striation-like features are also observed in the vacuum tested specimen, as seen in Figure 12c.

The alpha + beta solutioned material, on the other hand shows no grain features, as seen in Figure 13a. The basic fracture morphology in air is brittle, Figure 13b. Secondary cracking and striations are also seen, as in Figure 13c. The continuity of striations on either side of the secondary



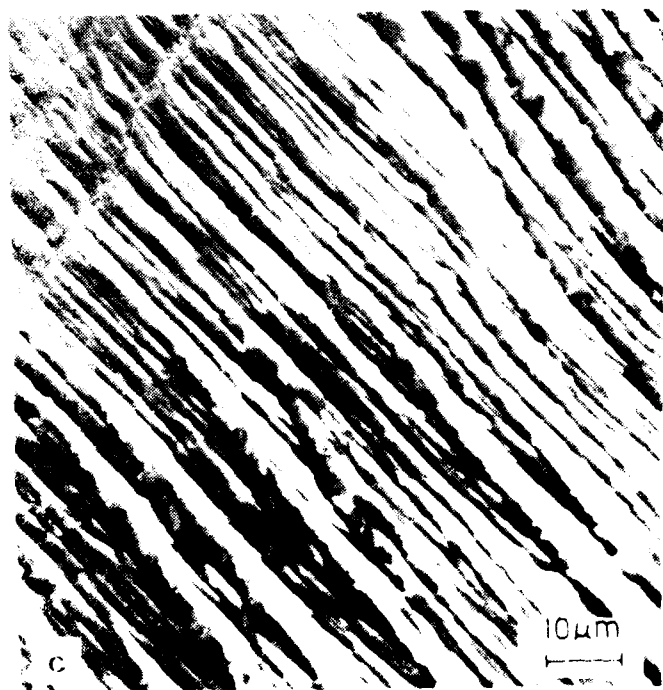


Figure 11 SEM fractographs of beta solutioned  $Ti_3Al$  fatigue crack growth specimen tested in air at 1200 F.

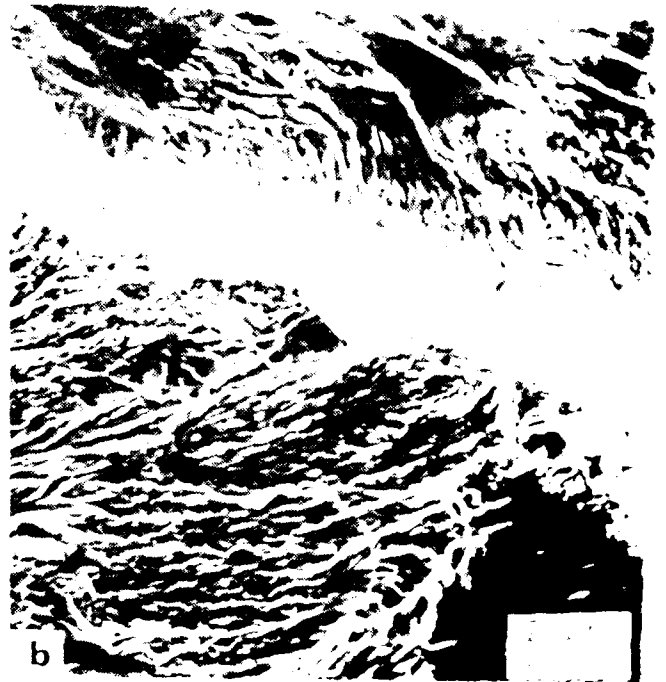


Figure 1. Scanning electron micrographs of the surface of the polyimide film. (a) shows the surface morphology of the polyimide film after 10 min of UV irradiation. (b) shows the surface morphology of the polyimide film after 30 min of UV irradiation. (c) shows the surface morphology of the polyimide film after 60 min of UV irradiation.



Figure 1b SEM of a cross-section of the fiber showing the internal structure.

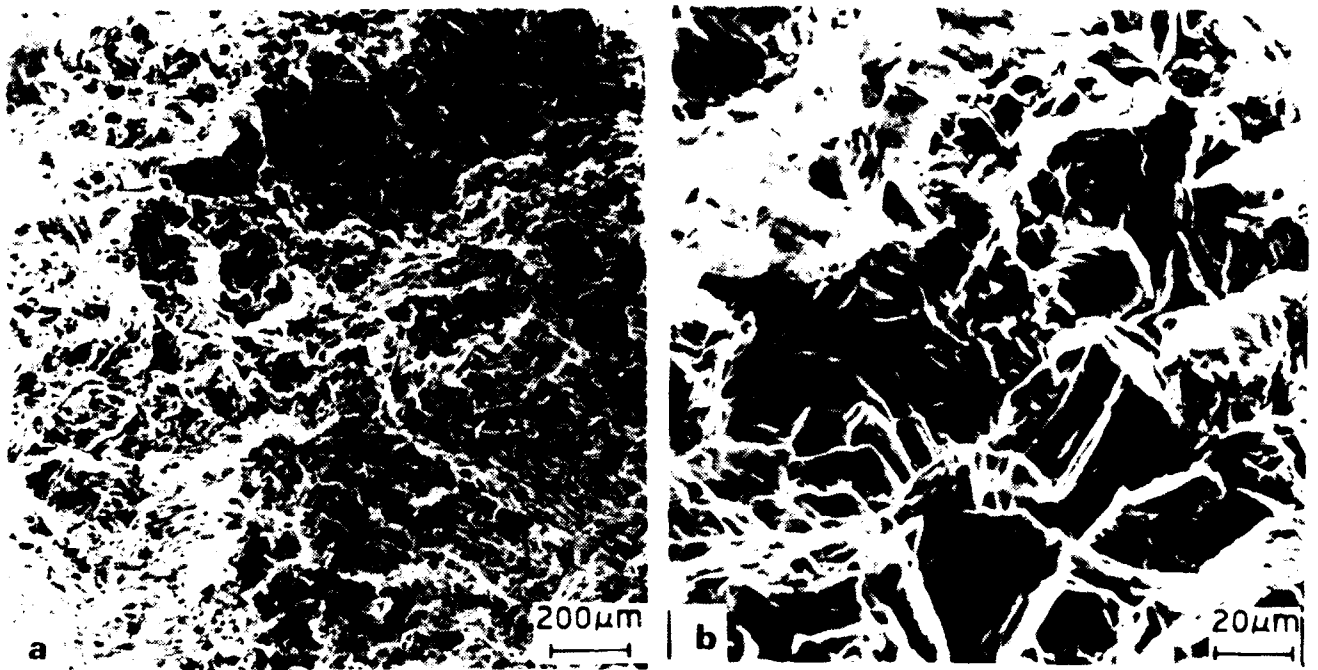


Figure 14 SEM fractographs of alpha + beta solutioned  $Ti_3Al$  fatigue crack growth specimen tested in vacuum at  $1200^{\circ}F$ .

crack indicate subsequent secondary cracking in this material. Figures 14a and 14b indicates a slight amount of plasticity on the fracture surface of the vacuum tested specimen, which is much less when compared to that found in beta solutioned material.

Hence, unlike superalloys where a change from an intergranular fracture morphology in air to a transgranular fracture morphology in the vacuum environment is observed, the alpha two titanium aluminide fails by the same transgranular fracture mode both in air and vacuum except for an increased plasticity in vacuum environment.

Figure 15 illustrates the fatigue crack growth data ( $da/dN$  vs  $\Delta K$ ) obtained at 1000°F (538°C). Major features are similar to those found at 1200°F (649°C) except that the beta solutioned material showed slightly lower growth rates in air in the low  $\Delta K$  regime. After analyzing the closure data given in Figures 16 and 17, and plotting the growth rate versus effective stress intensity range (Figure 18), however, this variation is reduced. Crack growth rates in vacuum are still much lower when compared to that in air for both heat treatments indicating an embrittlement of the material in air at this temperature.

Fractographs of specimens tested at 1000°F are shown in Figures 19 through 22. Beta solutioned material shows brittle fracture morphology (Figure 19a) with characteristic river patterns along the crack path as seen in Figure 19B. The vacuum tested specimen again showed considerable plasticity as seen in figures 20a and 20b. The extent of plastic work is vivid in figure 20c. Further, grain boundary cracking, prominent in 1200°F test samples is not observed at this temperature. This characteristic, along with the much improved ductility in vacuum, might be responsible for the lowest crack growth rates observed at this temperature in vacuum

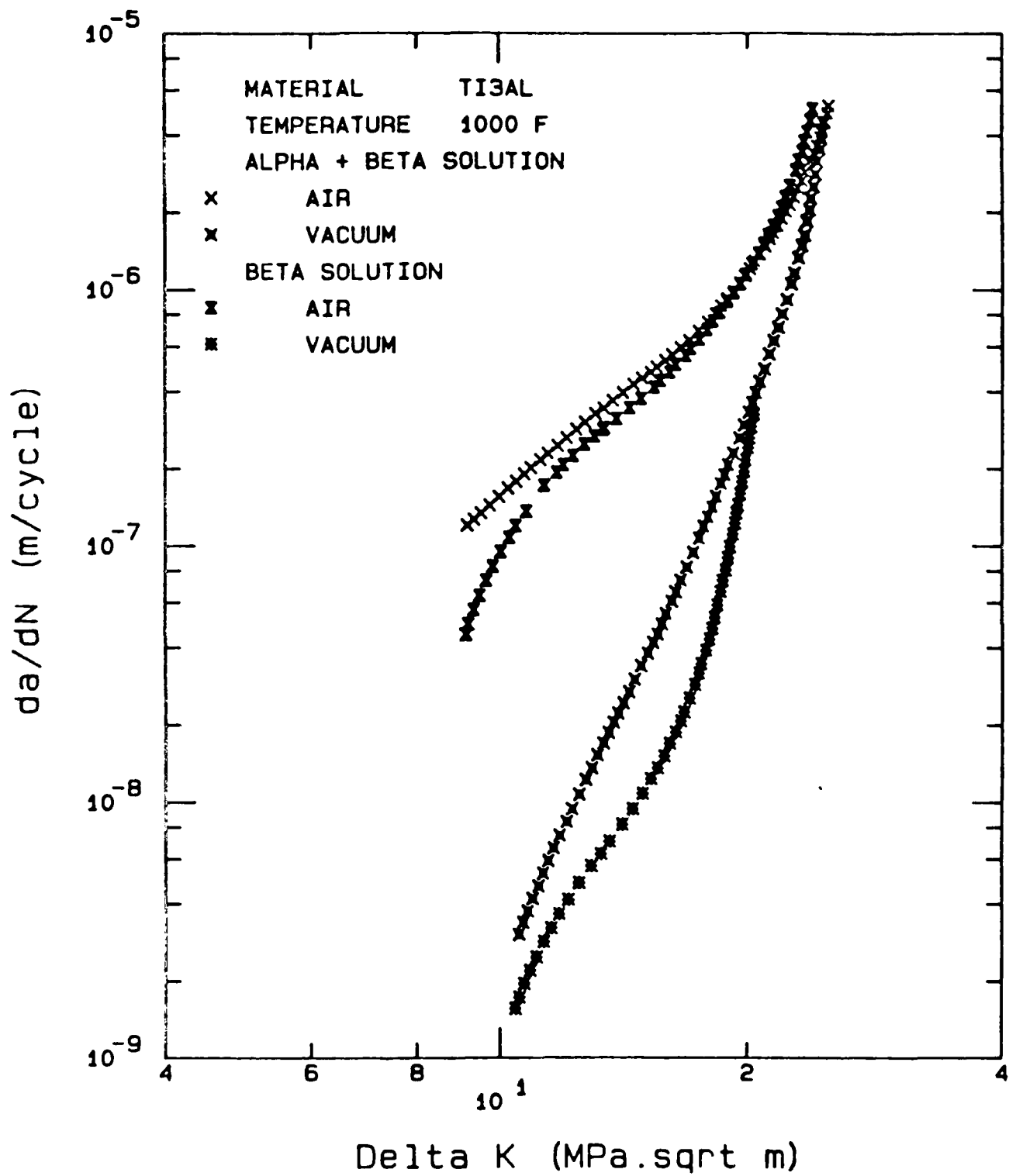


Figure 15 Fatigue crack growth data obtained for  $Ti_3Al$  at the temperature of  $1000^{\circ}F$ .

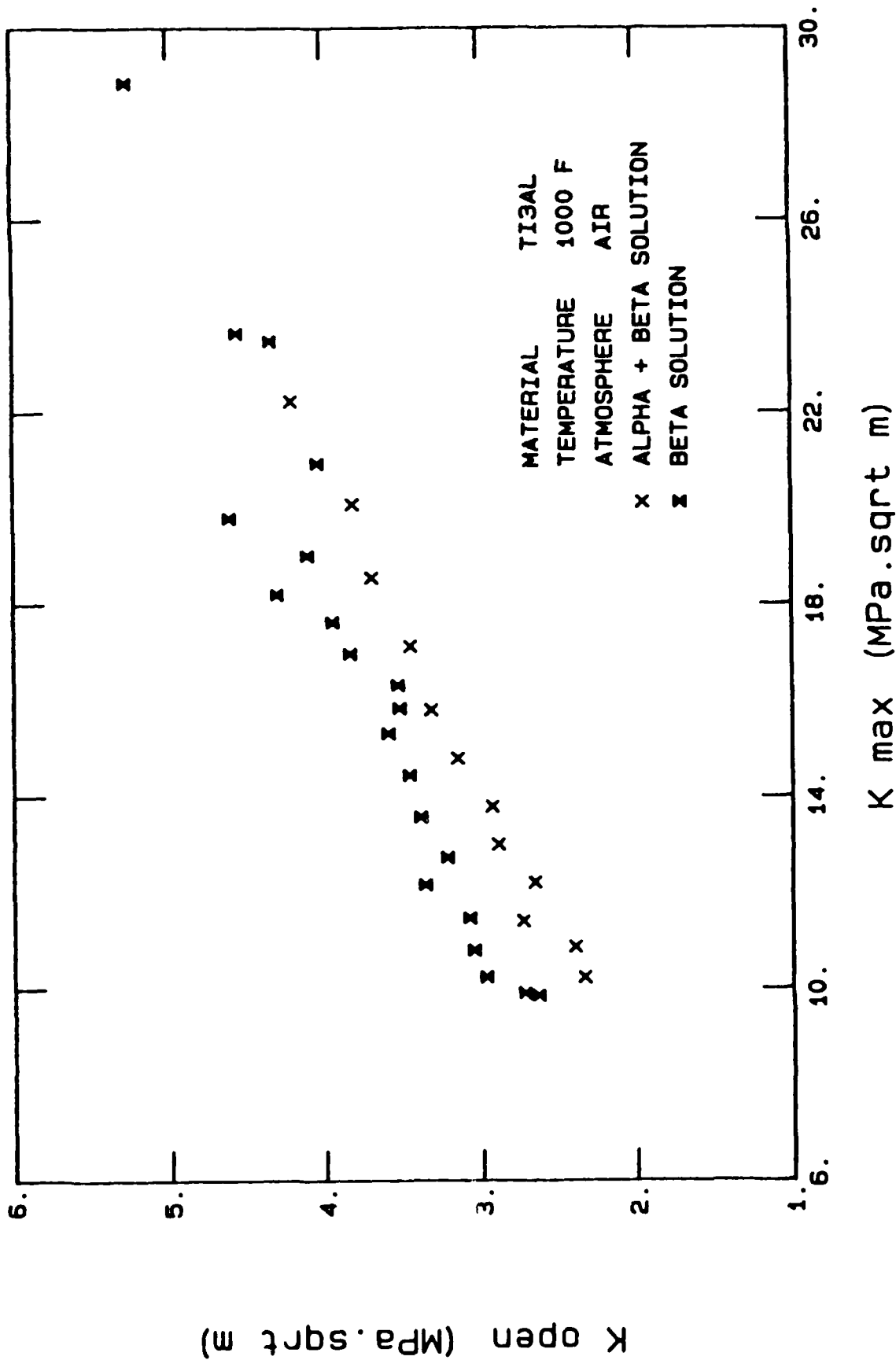


Figure 16 Closure data obtained for Ti<sub>3</sub>Al at the temperature of 1000°F in air environment.

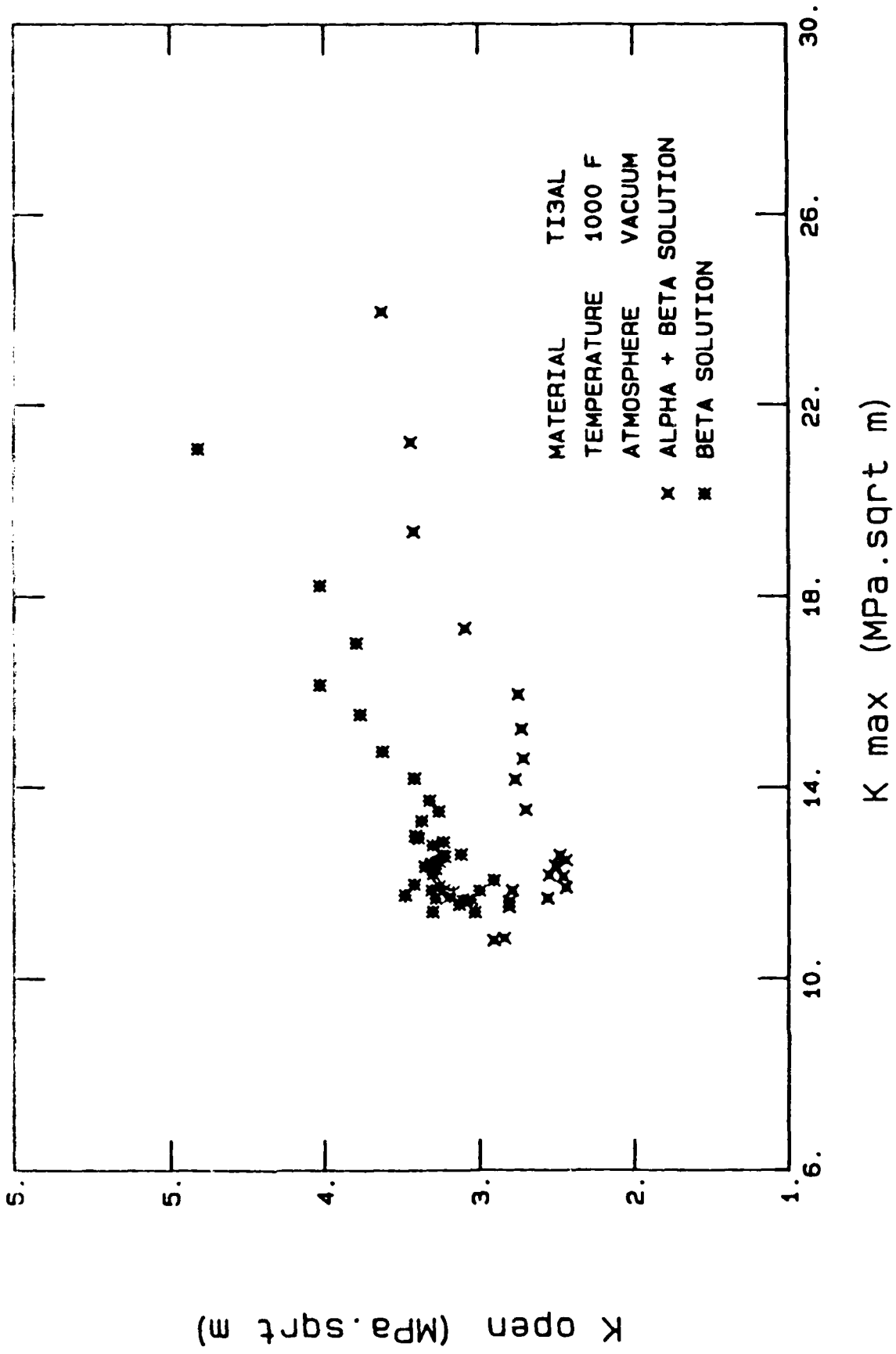


Figure 17 Closure data obtained for Ti<sub>3</sub>Al at the temperature of 1000°F in vacuum environment.



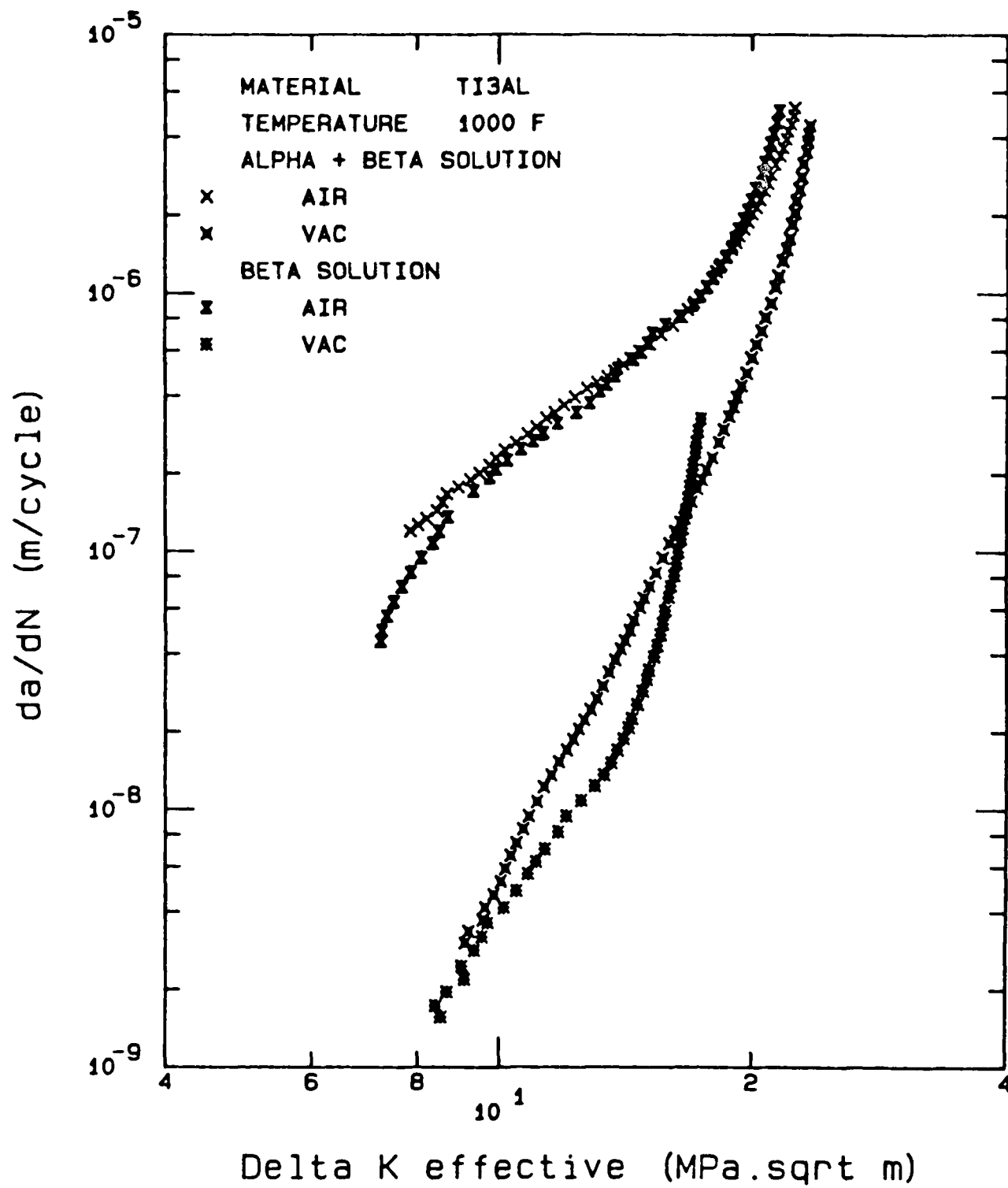


Figure 18 Closure corrected fatigue crack growth data for  $Ti_3Al$  obtained at the temperature of  $1000^\circ F$ .

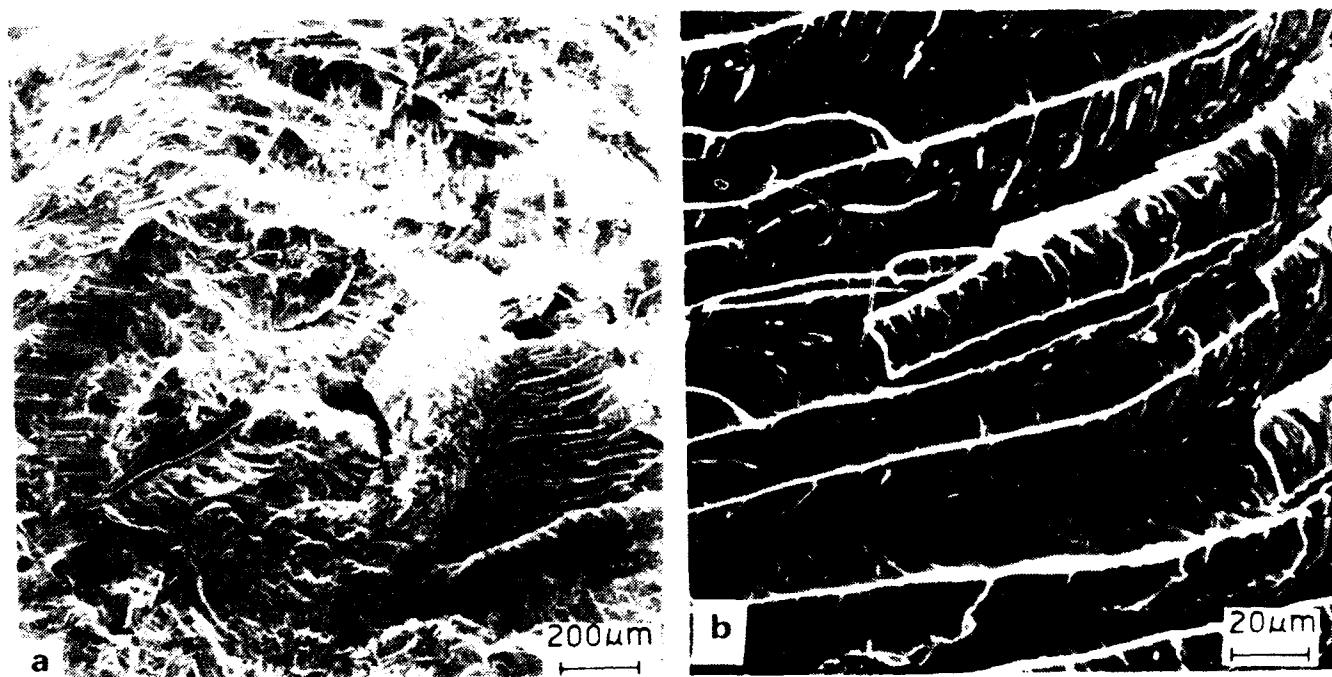


Figure 19 SEM fractographs of beta solutioned  $Ti_3Al$  fatigue crack growth specimen tested in air environment at 1000°F.

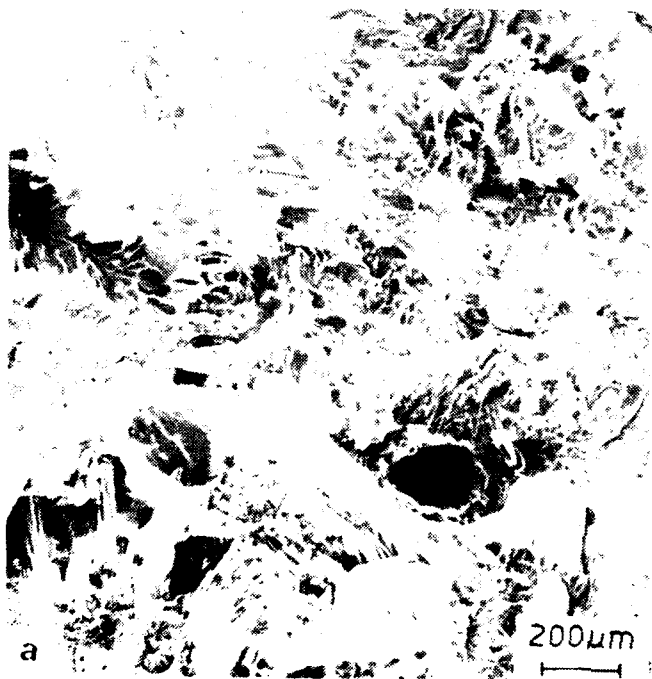


Figure 20 SEM fractographs of beta solutioned  $\text{Ti}_3\text{Al}$  fatigue crack growth specimen tested in vacuum at 1000°F.

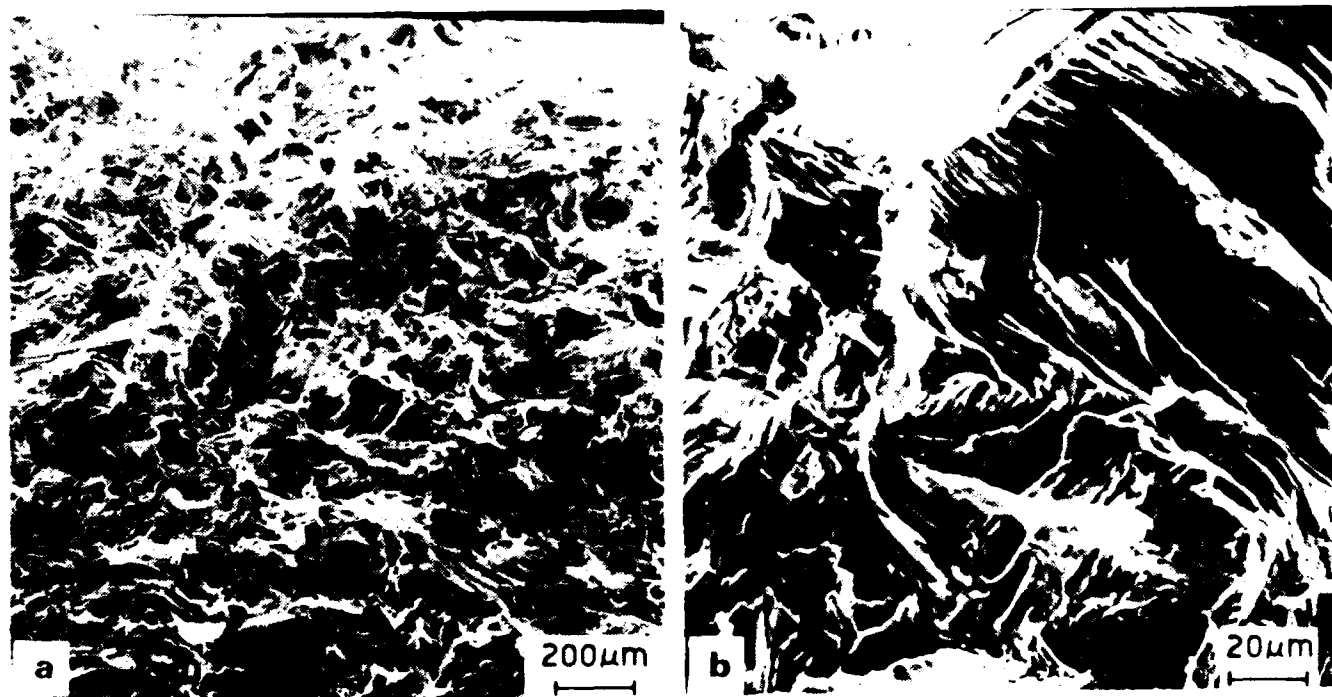


Figure 21 SEM fractographs of alpha + beta solutioned  $Ti_3Al$  fatigue crack growth specimen tested in air at  $1000^{\circ}F$ .

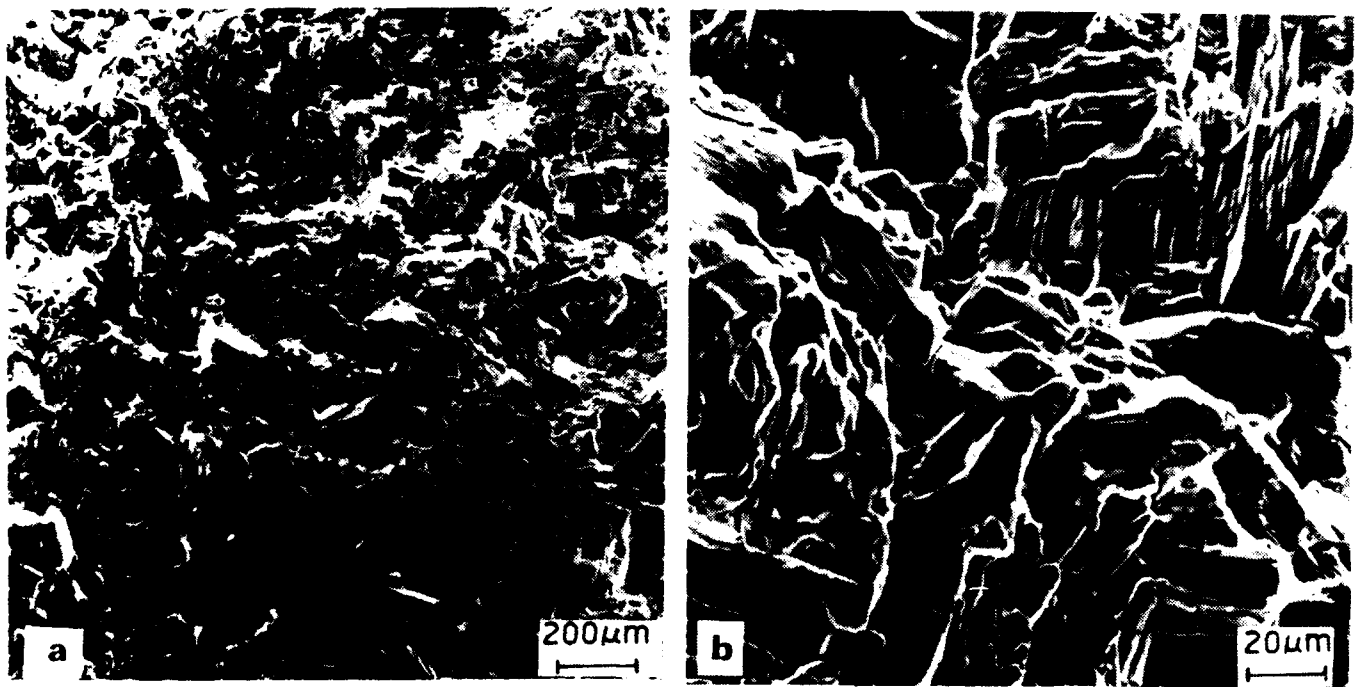


Figure 22 SEM fractographs of alpha + beta solutioned  $Ti_3Al$  fatigue crack growth specimen tested in vacuum at  $1000^{\circ}F$ .

environment.

Alpha + beta solutioned material shows brittle fracture morphology in both air and vacuum (Figures 21 and 22) with a limited amount of plasticity in vacuum tested specimens. These features are comparable to those observed at 1200°F.

The crack growth data obtained at 800°F (426°C) and 600°F (316°C) for both heat treated conditions are given in Figures 23 and 24. The material still shows considerable toughness. A crossover in the data indicated slower growth rates for beta solutioned material at low  $\Delta K$  regions. The closure data (Figures 25 and 26) obtained at these temperatures still showed higher levels of closure in beta solutioned alloy when compared to those in alpha + beta solutioned material. The growth rate vs effective stress intensity range data shown in Figures 27 and 28 eliminates the crossover in the data in the low  $\Delta K$  regime. Again, the closure levels are not high enough to influence the crack growth data markedly.

Finally, the room temperature crack growth data are given in Figure 29. Again, a crossover in the data showing lower growth rates for beta solutioned alloy is observed. The closure data shown in Figure 30 illustrates higher closure levels in beta solutioned alloy. No evidence of plasticity induced closure was observed in either heat treated condition. The  $da/dN$  vs  $\Delta K_{\text{effective}}$  data shown in Figure 31 is similar to that in Figure 29 except for a shift to the left. Further, the growth rate curves were quite steep indicating low fracture toughness values for the material at room temperature. This is due to limited ductility at this temperature arising from the restricted planar slip activity. Yet, it showed a steady state crack growth over the stress intensity range tested and improvements in alloy chemistry and microstructure should be able to enhance the room temperature properties further. This will be addressed in the Phase II

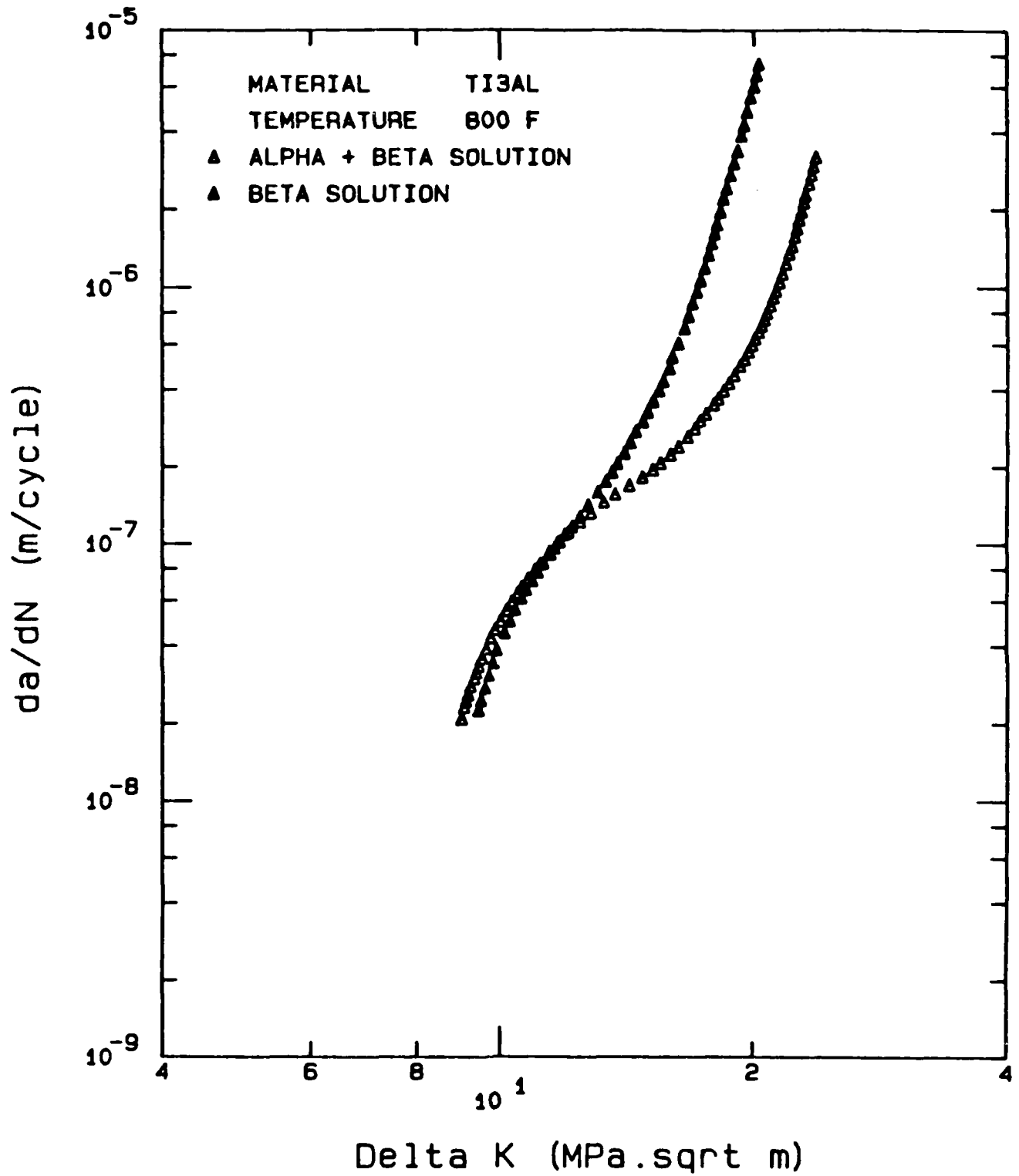


Figure 23 Fatigue crack growth data obtained for  $Ti_3Al$  at the temperature of 800°F.

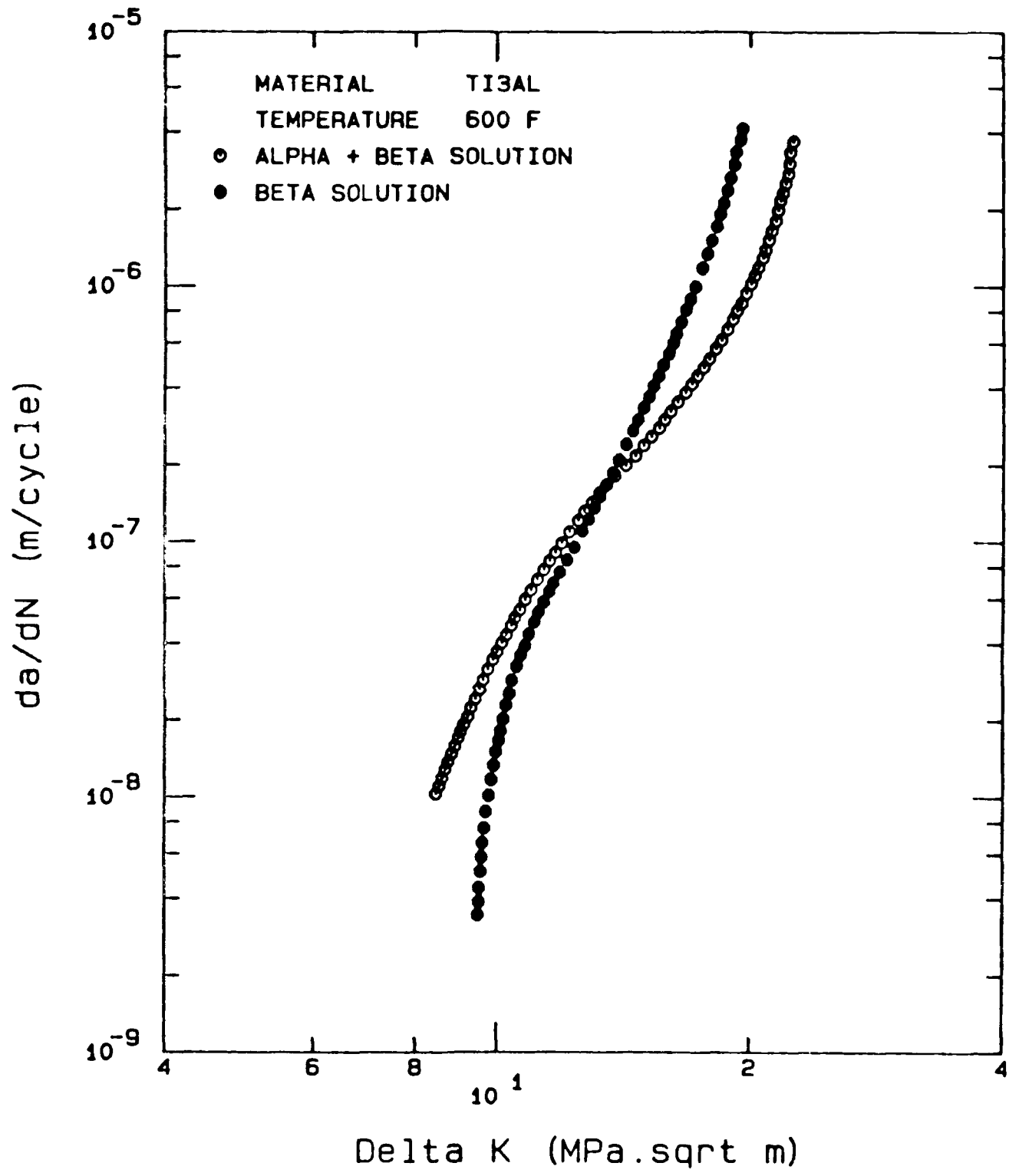


Figure 24 Fatigue crack growth data obtained for  $Ti_3Al$  at the temperature of 600°F.



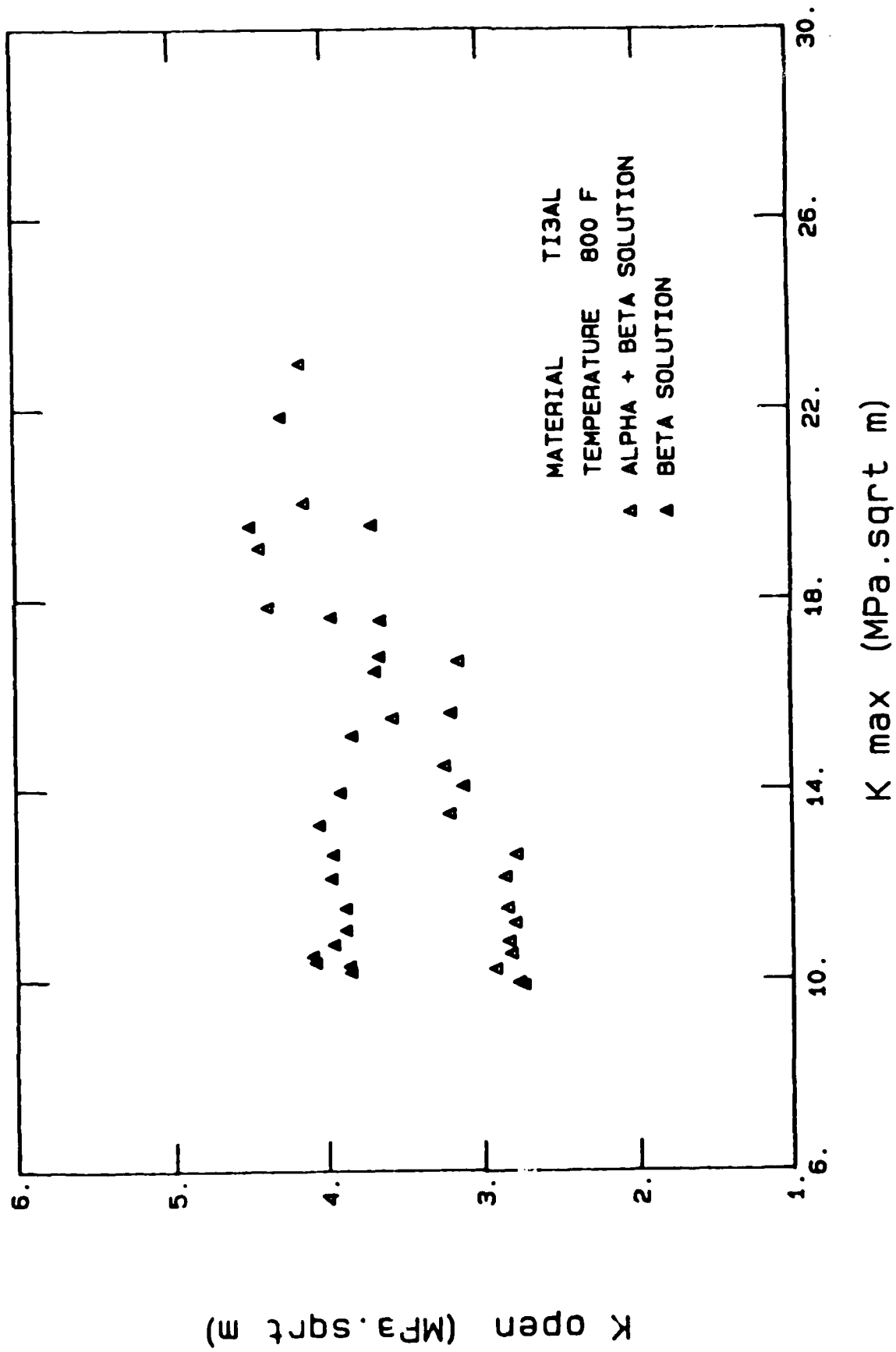


Figure 25 Closure data obtained for Ti<sub>3</sub>Al at the temperature of 800°F in air environment.

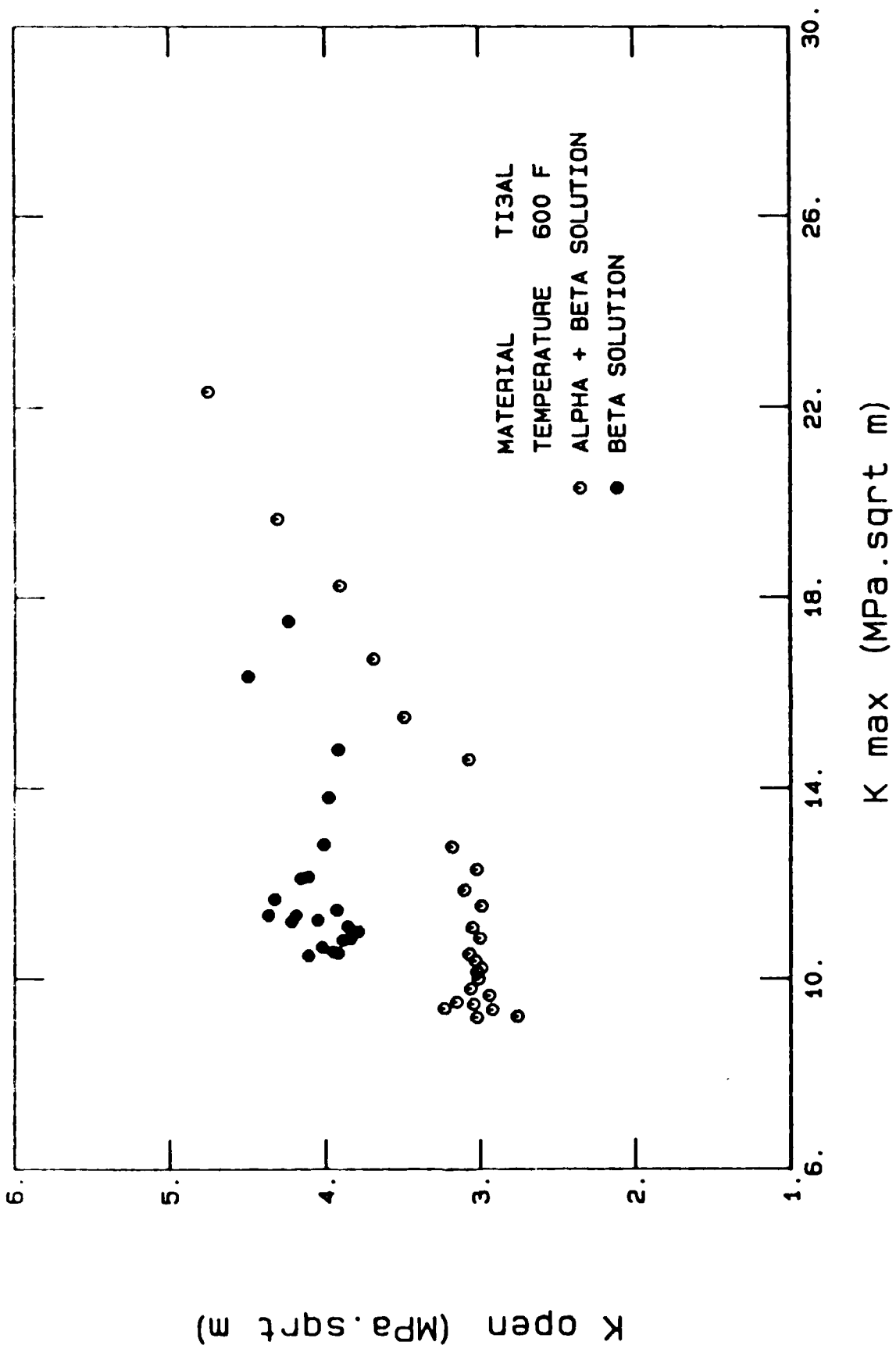


Figure 26 Closure data obtained for Ti<sub>3</sub>Al at the temperature of 600°F in air environment.

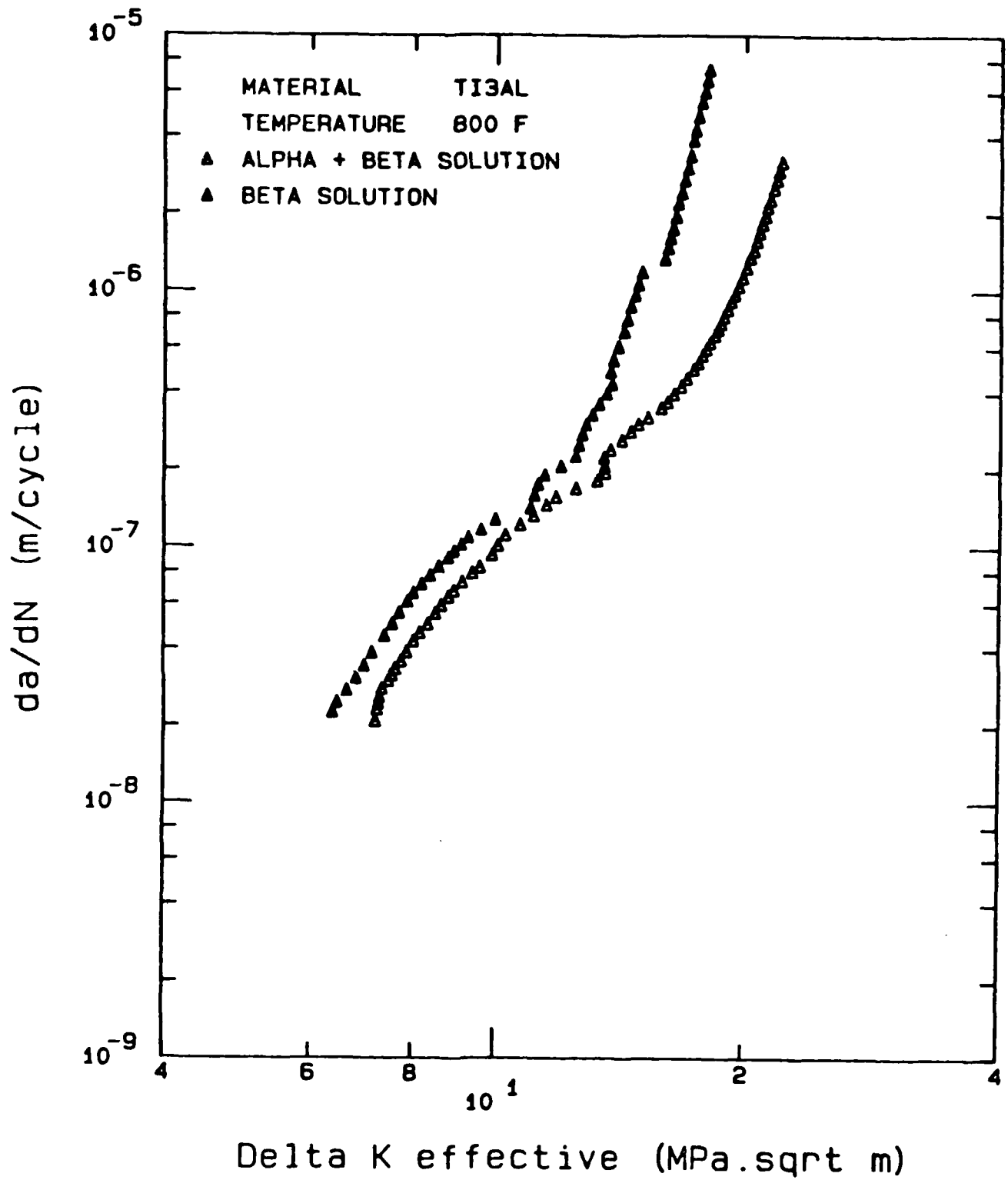


Figure 27 Closure corrected fatigue crack growth data for  $Ti_3Al$  obtained at the temperature of 800°F.

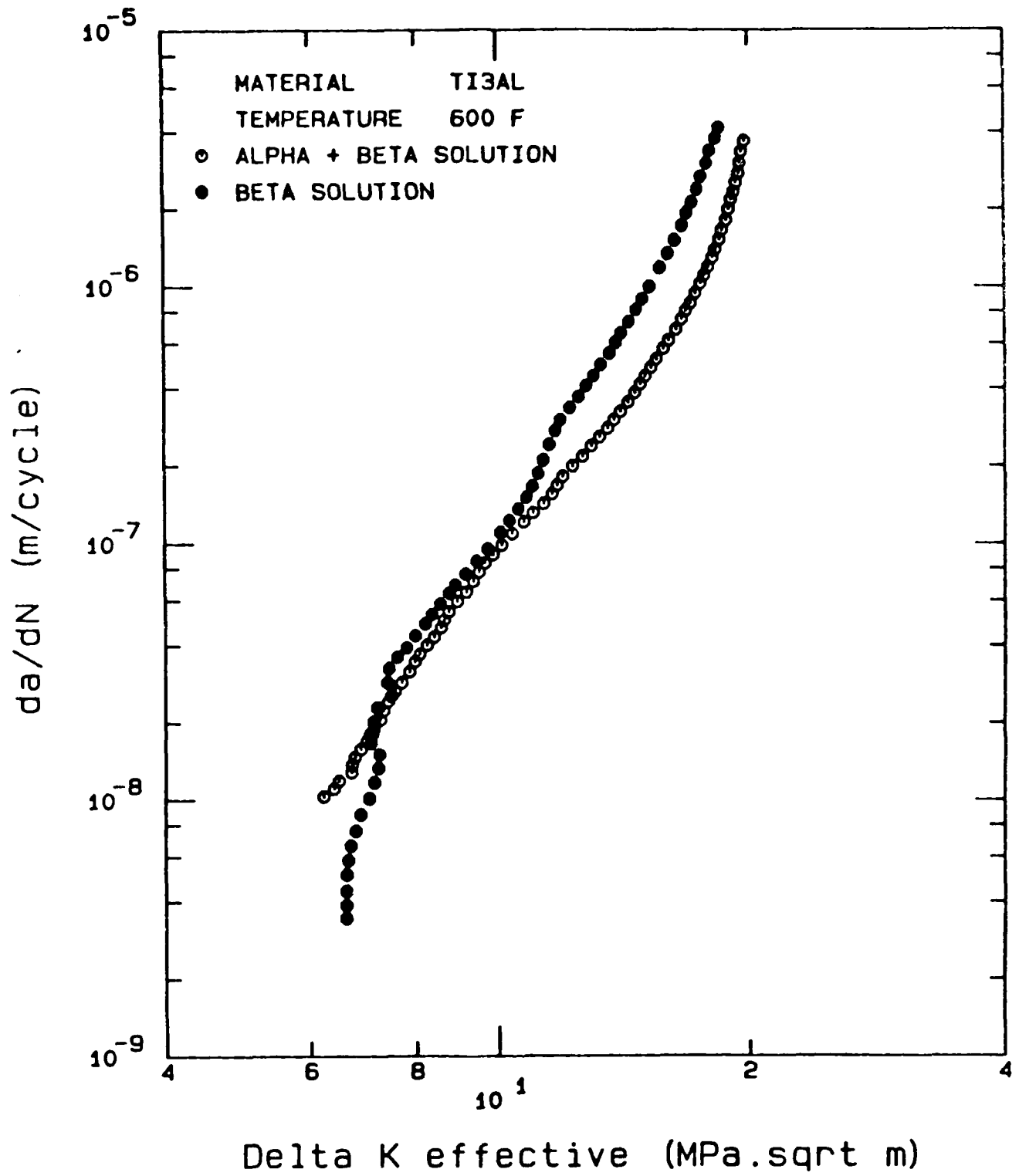


Figure 28 Closure corrected fatigue crack growth data for  $Ti_3Al$  obtained at the temperature of  $600^\circ F$ .

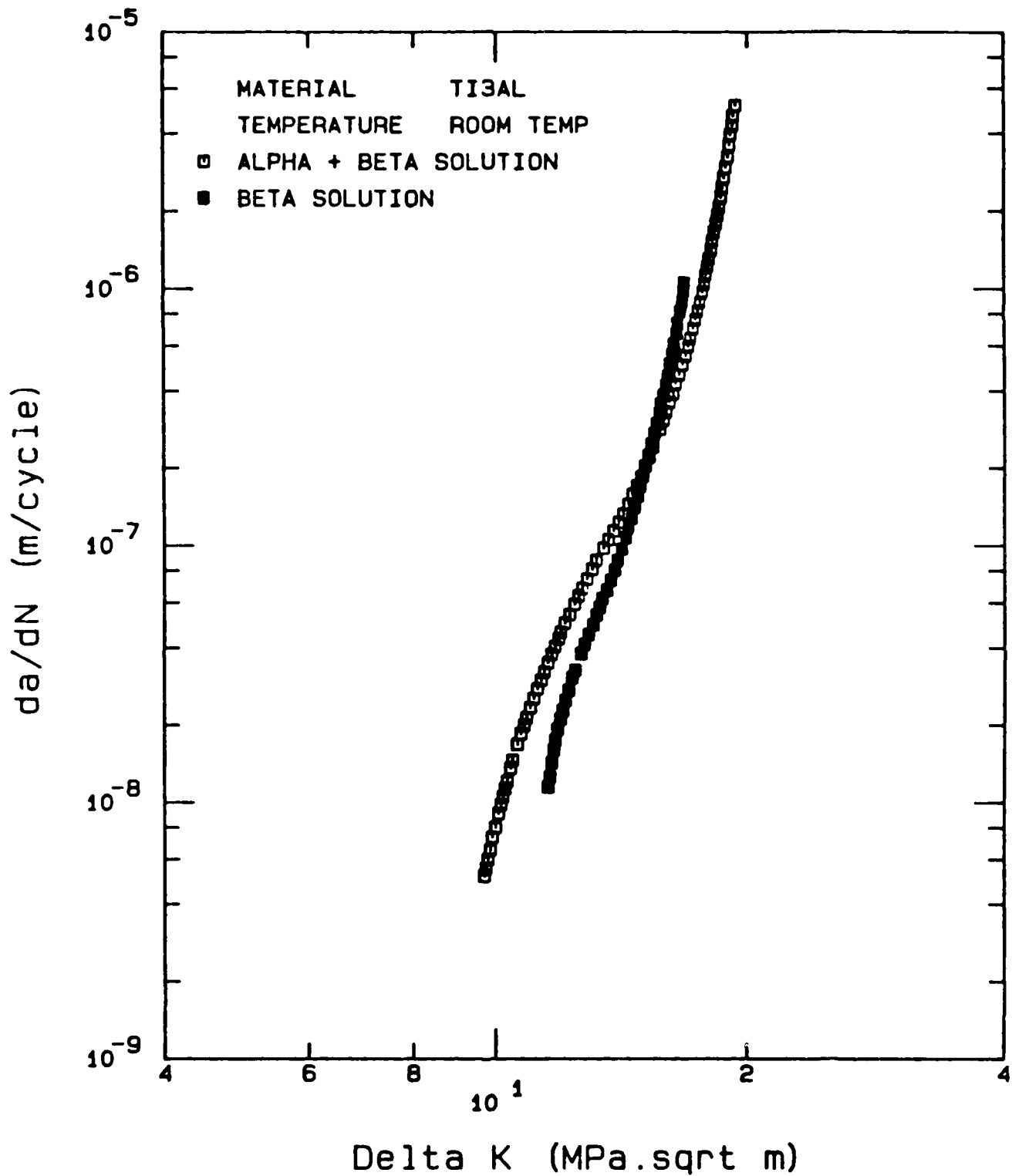


Figure 29 Fatigue crack growth data obtained for  $Ti_3Al$  at the temperature of 75°F (room temp).

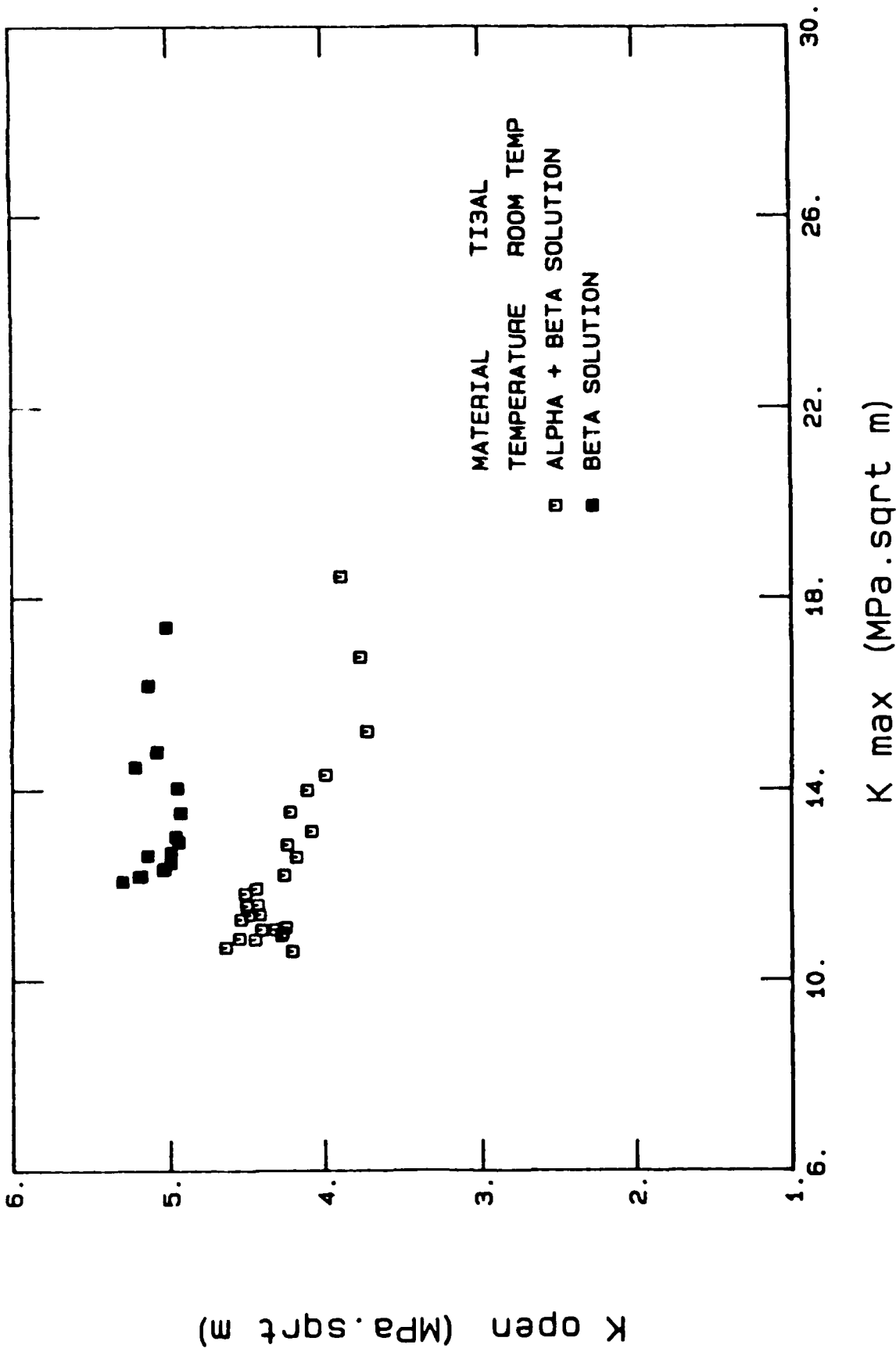


Figure 30 Closure data obtained for Ti<sub>3</sub>Al at the temperature of 75°F (room temp) in air environment.

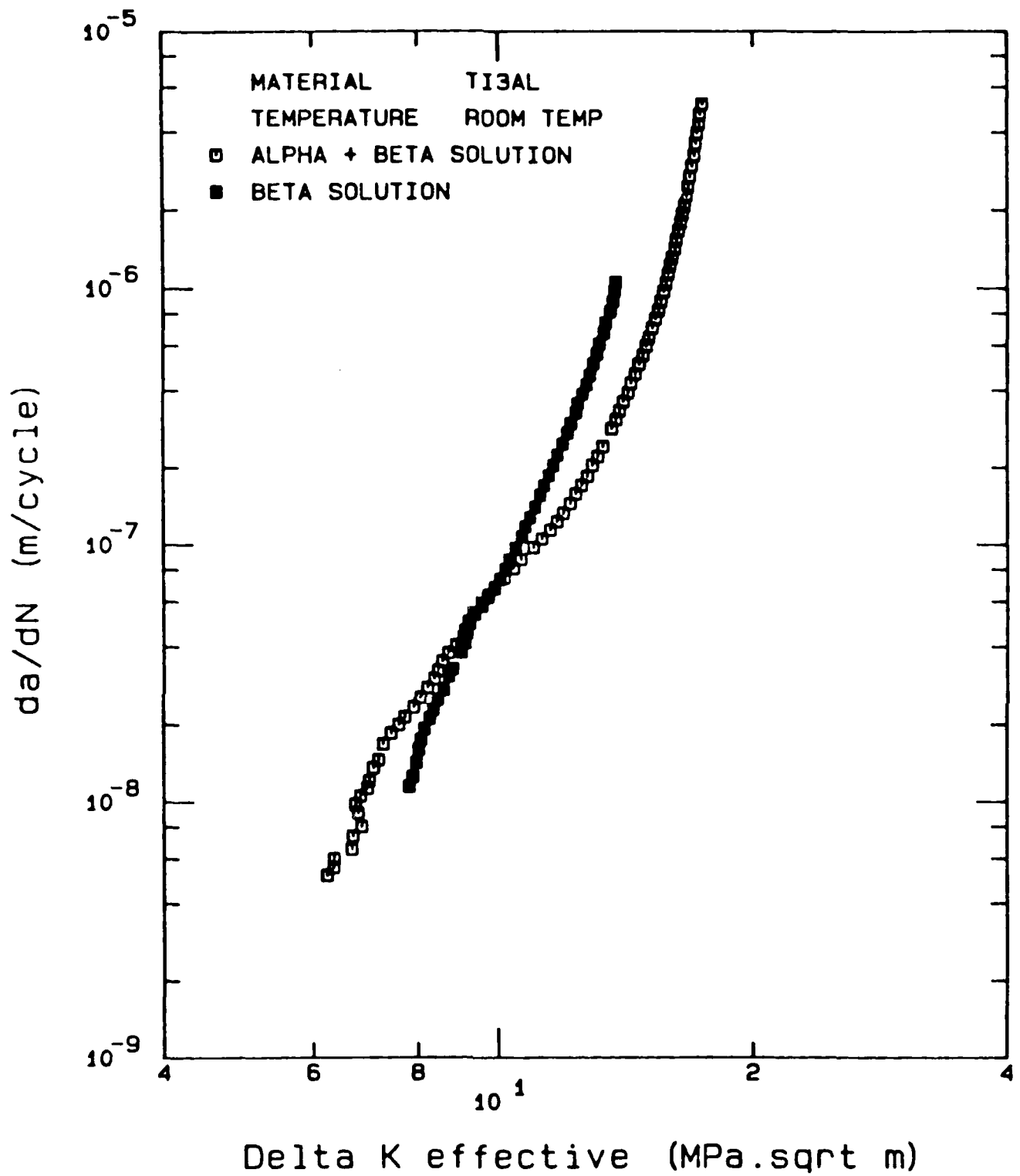


Figure 31 Closure corrected fatigue crack growth data for  $Ti_3Al$  obtained at the temperature of 75°F (room temp).

research program.

Fractographs of specimens tested at room temperature are shown in Figures 32 and 33. As is to be expected from the crack growth data, the fracture morphology was brittle in both cases. Grain features are visible in Figure 32a for beta solutioned material while Figure 32b illustrates snapped fine scale microstructure. In alpha + beta solutioned alloy the fracture surface is flat with the least amount of deformation as seen in Figure 33.

Summaries of crack growth data for each heat treatment over the temperature range tested are shown in figures 34 and 35. A moderate increase in growth rate is observed in both cases with increase in temperature except for room temperature where the limited ductility results in the steep crack growth curves. Lowest growth rate is observed at 1000°F (538 °C) when tested in a vacuum environment, indicating a strong environmental interaction in the alpha two titanium aluminide.

#### CONCLUSIONS AND RECOMMENDATIONS:

The feasibility study conducted in this Phase I program successfully answers the major questions on the life limiting processes occurring in the titanium aluminide. They can be listed as follows:

A. Role of oxygen on crack growth: Higher crack growth rates observed in the air environment at temperatures of 1000°F and 1200°F when compared to those in vacuum indicates an embrittling effect of oxygen on this material. Secondary cracks are observed only on the fracture specimens tested in air. In addition, an increased ductility is observed on fracture surfaces when tested in vacuum environment. These characteristics indicate a strong



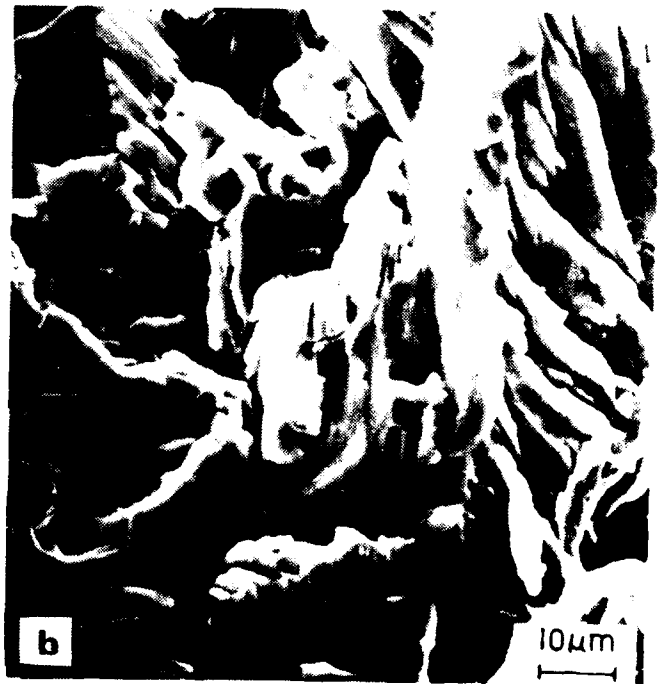


Figure 32 SEM fractographs of beta solutioned  $Ti_3Al$  fatigue crack growth specimen tested in air environment at 75°F (room temp).

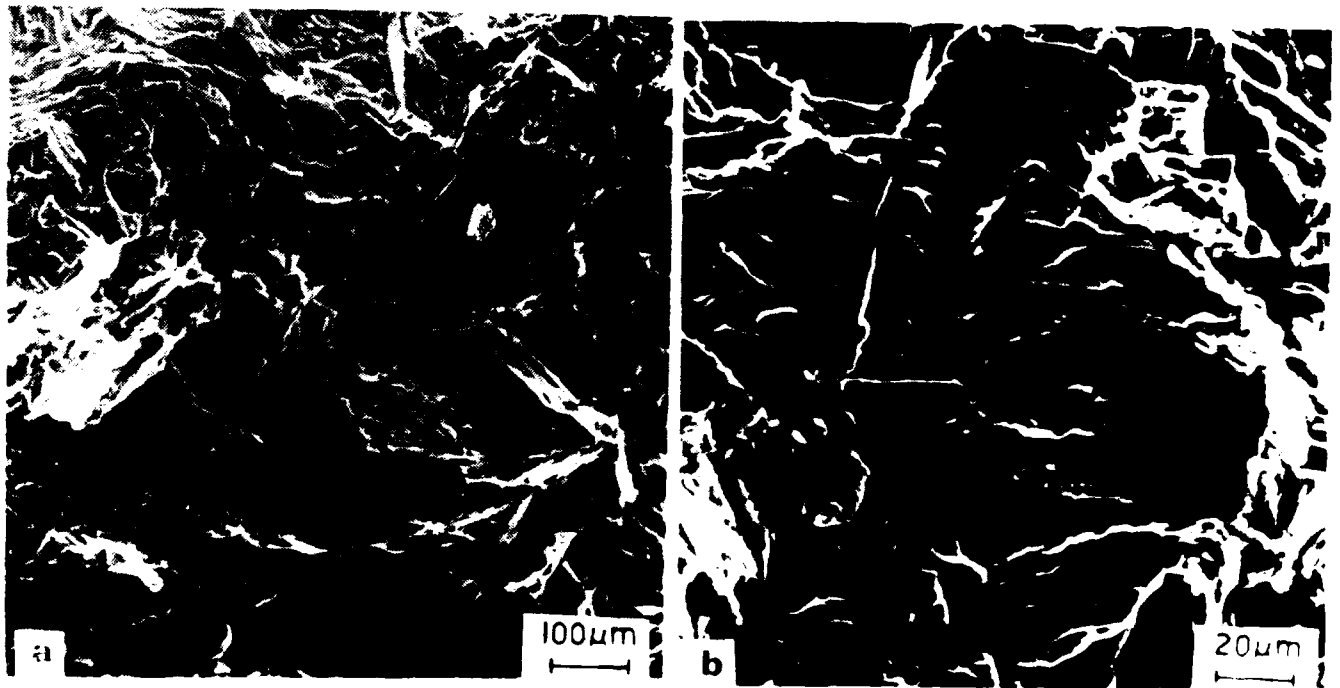


Figure 33 SEM fractographs of alpha + beta solutioned  $Ti_3Al$  fatigue crack growth specimen tested in air at 75 F (room temp).

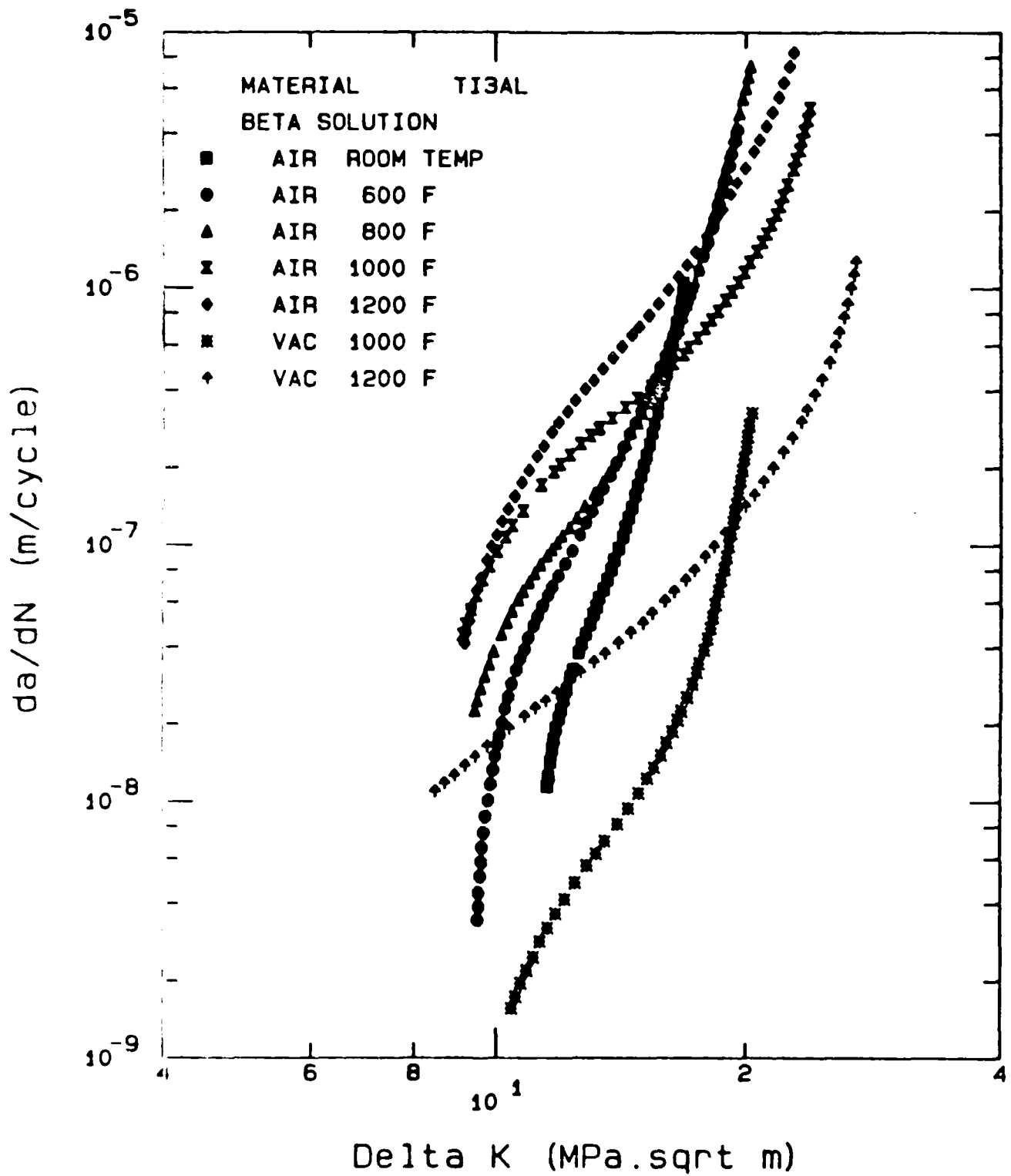


Figure 34 Summary of fatigue crack growth data obtained for the beta solutioned  $Ti_3Al$  over a temperature range of 75 to 1200°F in both air and vacuum environment.

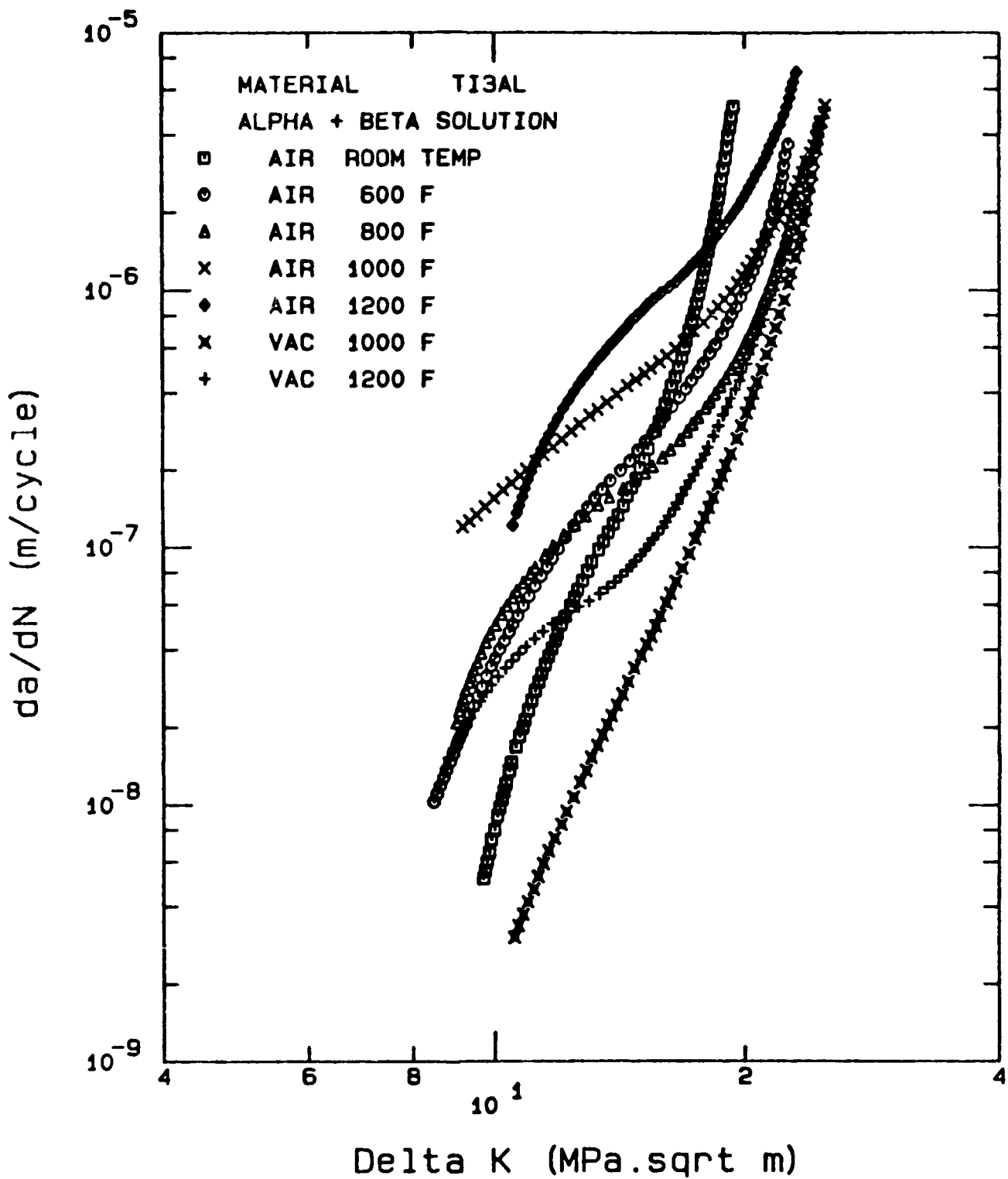


Figure 35 Summary of fatigue crack growth data obtained for the alpha + beta solutioned  $Ti_3Al$  over a temperature range of 75 to 1200°F in both air and vacuum environment.

influence of oxygen on the life limiting processes occurring in this material.

B. Role of temperature and ductility: The crack growth data obtained at the temperature of 600°F and over indicate fracture toughness values over 25 MPa√m showing increased ductility at elevated temperatures. Only a moderate increase in crack growth rates is observed with increase in temperature. The room temperature test data, however, shows limited ductility and toughness resulting in a steep crack growth curves.

C. Role of microstructure: The coarse grained beta solutioned microstructure shows an increased level of closure and slightly lower crack growth rates when compared to the fine grained alpha + beta solutioned alloy. The beta solutioned structure also showed increased plasticity on the fracture surfaces when tested in vacuum indicating a microstructure - environmental interaction.

The above mentioned results pave the way for a successful Phase II research program. The basic understanding of the crack growth behavior in the alpha two titanium aluminide obtained in this program should be extended to the most recent alloy, namely, titanium - 24 atom % aluminum - 11 atom % niobium alloy with improved ductility and toughness. The data obtained in Phase I should aid in choosing an experimental matrix for a detailed study of the life limiting processes in this alloy with respect to variables such as frequency, load amplitude, wave shape, hold time, environment, etc.

Increased beta phase stability due to higher niobium concentration in this material should be exploited to modify the material microstructure through heat treatment procedures so as to introduce high levels of closure. This should reduce the crack tip stress intensity, thus improving crack growth resistance of the alloy.

After gaining thorough understanding of the mechanical behavior of this improved alloy in its monolithic form and evaluating its applicability to various rotating engine components using the life prediction criteria, the potential for its application in a composite form should also be explored.

## REFERENCES

1. "Titanium Aluminides - An Overview," H. A. Lipsitt, Materials Research Society Symposium Proceedings, vol. 39, 1985.
2. "Research To Conduct An Exploratory Experimental And Analytical Investigation Of Alloys," Technical Report No. AFML-TR-78-18, Wright-Patterson Air Force Base, March, 1978.
3. "Metallides, A New Base For Heat-Resistant Materials," I. I. Kornilov, 'Structure And Properties Of Heat Resistant Metal Materials', Svoystva Zharoprochynkh Metallicheskih Materialov, Moscow, Narka, 1967.
4. "Properties Of Alloys Based On The Aluminide  $Ti_3Al$ ," T. T. Nartova, Poroshkovaya Metallurgiya, No. 8 (44), pp. 43-48, 1966.
5. "The Deformation And Fracture Of  $Ti_3Al$  At Elevated Temperatures," H. A. Lipsitt, D. Shechtman, And R. E. Schafrik, Metallurgical Transactions A, vol 11A, August 1980, pp. 1369.
6. "Oxidation Resistance Of The Compound  $Ti_3Al$  And Its Alloys At Temperatures Of 700 And 800°C," I. A. Zelenkov and E. N. Osokin, Soviet Powder Metallurgy, Metals and Ceramics, October 14 (10), 1975, pp. 839.
7. "Steady-State Creep Behavior Of  $Ti_3Al$  - Base Intermetallics," M. G. Mendiratta, And H. A. Lipsitt, Journal Of Materials Science, 1980, pp. 2985.
8. "Ordering Transformations And Mechanical Properties Of  $Ti_3Al-Nb$  Alloys," S. M. L. Sastry, And H. A. Lipsitt, Metallurgical Transactions A, vol. 8A, October 1977, pp. 1543.
9. "Life Prediction For Turbine Engine Components," T. Nicholas, And J. M. Larsen, 'Fatigue: Environment And Temperature Effects', Proceedings Of The 27th Sagamore Army Materials research Conference, 1980, pp. 353.
10. "An Automated Photomicroscopic System For Monitoring The Growth Of Small Fatigue Cracks," J. M. Larsen, To Be Published In ASTM-STP Of ASTM

Seventeenth National Symposium On Fracture Mechanics August 1984.

11. C. T. Liu, C. L. White And E. H. Lee, *Scripta Metallurgica*, Vol. 19, pp. 1247, 1985.



EMD

DATE

FILMED

3-88

DTIC